ELSEVIER

Progress in Nuclear Magnetic Resonance Spectroscopy 53 (2008) 105–127

PROGRESS IN NUCLEAR MAGNETIC RESONANCE SPECTROSCOPY

www.elsevier.com/locate/pnmrs

In situ flow MAS NMR spectroscopy: State of the art and applications in heterogeneous catalysis

Michael Hunger *

Institute of Chemical Technology, University of Stuttgart, 70550 Stuttgart, Germany

Received 2 July 2007; accepted 28 August 2007
Available online 12 September 2007

Keywords: *In situ* solid-state NMR spectroscopy; Flow technique; Porous solids; Heterogeneous catalysis

Contents

1. Introduction . . . 106
2. Experimental techniques . . . 106
   2.1. Flow MAS NMR probes . . . 106
   2.2. Peripheral equipment and protocols of flow MAS NMR experiments . . . 108
   2.3. MAS NMR-UV/Vis technique . . . 110
   2.4. Application of hyperpolarized xenon in flow MAS NMR spectroscopy . . . 111
   2.5. Temperature behavior of *in situ* MAS NMR probes . . . 111
3. ^{129}Xe MAS NMR spectroscopic investigations of the pore system of solid catalysts using hyperpolarized xenon under continuous-flow conditions . . . 112
   3.1. Studies of the pore architecture of ITQ-6 . . . 112
   3.2. Real time studies of adsorption processes on porous catalysts . . . 114
4. Studies of the behavior of solid catalysts and of reaction mechanisms in heterogeneous catalysis by flow MAS NMR spectroscopy . . . 114
   4.1. Coordination change of zeolitic framework atoms upon continuous hydration and dehydration . . . 114
   4.2. Hydrogenation of toluene on Pt/ZrO_2–SO_4 . . . 116
   4.3. Synthesis of methyl-*tert*-butylether on acidic zeolite catalysts . . . 117
   4.4. Formation and decomposition of N,N,N-trimethylanilinium cations on acidic zeolite catalysts studied by stopped-flow experiments . . . 118
5. Application of *in situ* flow MAS NMR-UV/Vis spectroscopy for the study of reaction mechanisms and organic deposits on solid catalysts . . . 120
   5.1. H/D exchange at the side-chain of ethylbenzene on acidic zeolite catalysts investigated by pulsed-flow experiments . . . 120
   5.2. Organic deposits formed on H-SAPO-34 during the methanol-to-olefin conversion . . . 122
   5.3. Quantitative investigations of the regeneration of coked MTO catalysts . . . 123
6. Conclusions . . . 125
   Acknowledgements . . . 126
   References . . . 126

* Tel.: +49 711 685 64079; fax: +49 711 685 64081.
E-mail address: michael.hunger@itc.uni-stuttgart.de

0079-6565/$ - see front matter © 2007 Elsevier B.V. All rights reserved.
doi:10.1016/j.pnmrs.2007.08.001

1. Introduction

In 1987 the first *in situ* solid-state NMR investigations of heterogeneously catalyzed reactions under continuous-flow conditions were performed [1,2]. These experiments were carried out without application of the MAS technique, which limited the spectral resolution and interpretation of spectra. During the past decade, a number of new experimental techniques have been developed for investigating working catalysts via MAS NMR spectroscopy under flow conditions. Nowadays, these approaches are called *operando* techniques [3,4], if the working catalyst is situated inside the spectroscopic equipment, i.e., in the present case, inside a high-temperature MAS NMR probe und utilizing the MAS NMR rotor as a microreactor. In some cases, *in situ* flow MAS NMR spectroscopy is coupled with analytical methods, such as gas chromatography or mass spectrometry. MAS NMR spectroscopy allows the study of the framework and surface sites of solid catalysts and of the adsorbate complexes on these materials under reaction conditions. On-line analysis of the exhaust gas gives additional information about volatile reaction products.

Generally, *in situ* flow MAS NMR spectroscopy is utilized for clarifying:

(i) the nature, behavior, and transformation of surface sites on solid catalysts under reaction conditions;
(ii) adsorption processes on porous solids;
(iii) the nature of surface complexes formed by adsorption of reactants;
(iv) the nature and reactivity of intermediates formed on the active sites of solid catalysts;
(v) the nature and reactivity of deposits on solid catalysts under steady-state conditions, and
(vi) the reasons for catalyst deactivation.

The above-mentioned investigations give new insights into the principles of working solid catalysts and improve our knowledge and understanding of the mechanisms of heterogeneously catalyzed reactions. The following contribution is a survey of the state of the art of experimental techniques developed and utilized for *in situ* MAS NMR spectroscopy under flow conditions. By examining characteristic examples, the possibilities of these modern spectroscopic approaches for investigations in the field of heterogeneous catalysis are demonstrated. For further information, the reader is directed to Refs. [5–8].

2. Experimental techniques

2.1. Flow MAS NMR probes

An often utilized approach for *in situ* MAS NMR investigations of heterogeneously catalyzed reactions under flow conditions is based on the injection of carrier gas (e.g., nitrogen) loaded with vapors of reactants into the spinning MAS NMR rotor via an injection tube [9,10]. For this purpose, a tube made of glass or ceramics is inserted into the sample volume of an MAS NMR rotor *via* an axially placed hole in the rotor cap (Fig. 1). The catalyst is shaped to a hollow cylinder and rotates with the rotor. The injection tube is fixed by a support and so a gap is required between the catalyst bed and the injection tube.

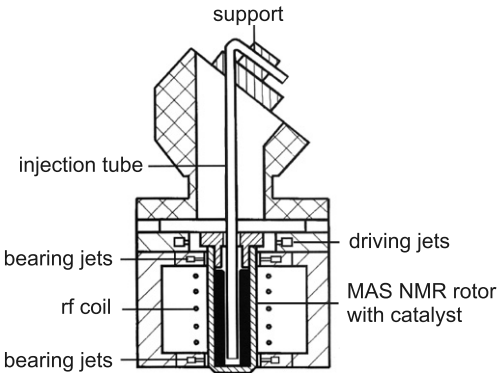


Fig. 1. The upper part of the first *in situ* MAS NMR probe equipped with an injection tube for experiments under flow conditions [9].

The reactants are injected into the inner space of the cylindrical catalyst bed and flow from the bottom to the top of the sample volume inside the MAS NMR rotor reactor. The product stream leaves the sample volume via an annular gap in the rotor cap (Fig. 2). In some cases, an additional tube with a larger diameter reaching into the rotor cap is used to suck off volatile reaction products leaving the rotor reactor at the annular gap [11]. In Fig. 2, this

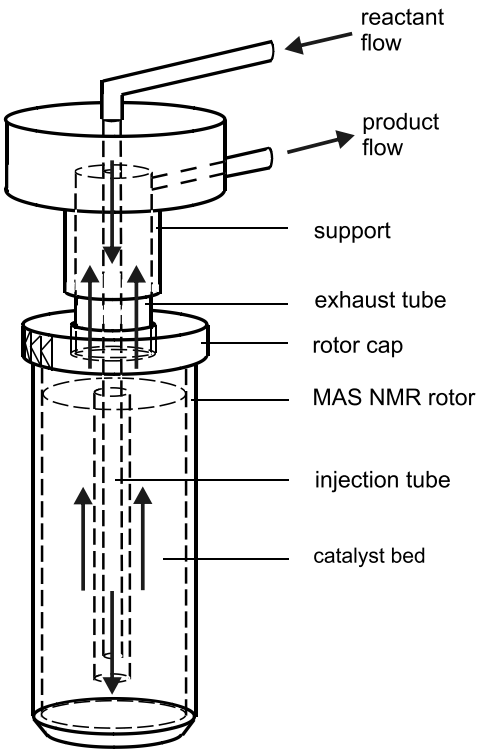


Fig. 2. The injection head of an *in situ* flow MAS NMR probe showing the reactant flow inside the MAS NMR rotor reactor and tubes (after Ref. [11]).

tube is called exhaust tube. The exhaust tube is connected with a pump feeding the reaction products to a peripheral analysis system, such as a gas chromatograph or mass spectrometer.

As described by Buchholz et al. [12], the injection tube of a modified 4 mm MAS NMR probe has an outer diameter of 1 mm, while the hole in the rotor cap has an inner diameter of 1.4 mm. This 4 mm MAS NMR probe reaches sample spinning frequencies of 12 kHz and is suitable for the investigation of ca. 50 mg of a dehydrated catalyst powder. Such a modified 4 mm MAS NMR probe was used, for example, for studying the framework and surface sites of solid catalysts during continuous hydration/dehydration and ammoniation/deammoniation cycles by ^{1}H and ^{27}Al MAS NMR spectroscopy [12,13].

In situ ^{13}C MAS NMR studies of reactants, organic adsorbate complexes, and deposits are performed with modified 7 mm MAS NMR probes with a much larger sample volume in comparison with 4 mm MAS NMR probes. The injection tube of the 7 mm MAS NMR probe has an outer diameter of 1.5–1.8 mm, while the hole in the rotor cap has an inner diameter of ca. 2.0 mm. The maximum sample spinning rate of 7 mm MAS NMR rotors is ca. 5 kHz. However, often spinning rates of 2–3 kHz are sufficient for the resolution of ^{13}C MAS NMR signals at elevated temperatures. In the 7 mm MAS NMR rotor, 100– 200 mg of catalyst powder can be filled. If an exhaust tube is added, it has a diameter of ca. 3 mm, while the axially placed hole in the rotor cap has an inner diameter of 3.2–3.5 mm [11].

Fig. 3a shows the special tool used for pressing the catalyst bed to form a hollow cylinder. Often, the shaping of the calcined and dehydrated catalyst is performed in a glove box purged with dry nitrogen gas. During the transfer of the MAS NMR rotor filled with dehydrated catalyst from the glove box to the flow MAS NMR probe, the axially placed hole in the rotor cap is sealed by a narrow strip of Tesa film. This strip is removed during nitrogen purging of the upper part of the probe, e.g., via the exhaust tube. With this procedure, a rehydration of the calcined catalyst powder during the sample transfer can be avoided. The probe in Fig. 3b is a modified 7 mm Bruker MAS NMR probe. The rotor lift at the top of the stator was replaced by a support for fixing the injection tube. This tube is bent by 90° because of the spatial limitations in the upper part of the probe. See Refs. [14–17] for further details concerning the construction of flow MAS NMR probes with similar or strongly modified injection systems. A limitation of flow MAS NMR probes with injection systems is the fact that the sample volume of these probes is not gas tight at the outlet of the reactant gas in the rotor cap. However, a contamination of the catalysts with impurities can be avoided, if dry carrier gas, such as dry nitrogen gas, is utilized for bearing and driving the MAS NMR rotor.

Flow MAS NMR probes allowing a total separation of the reactant flow and the gas used for driving the rotor are based on mechanical bearings [18–20]. The probe shown in

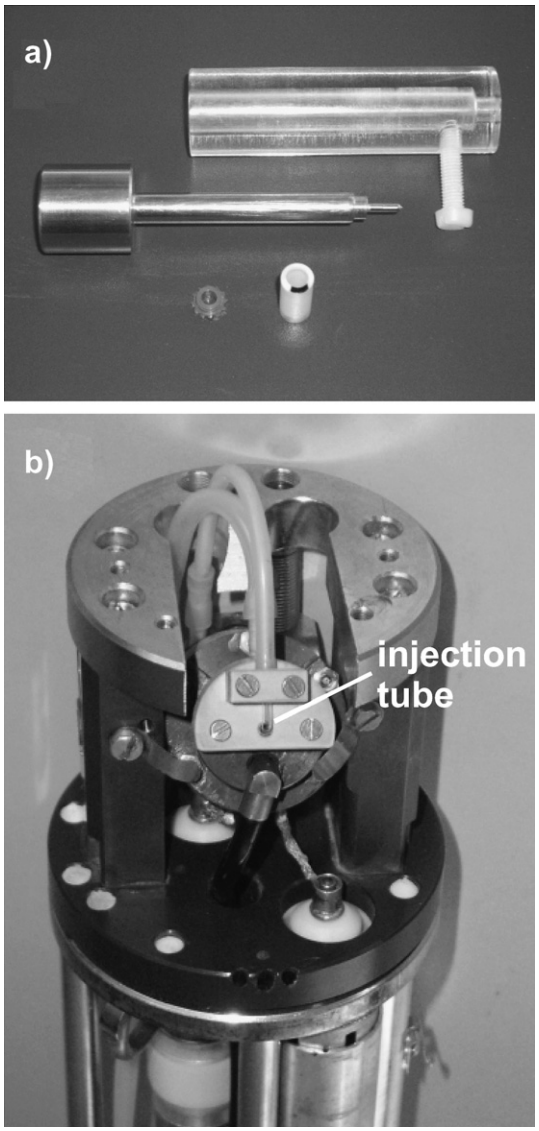


Fig. 3. The tools used for shaping the catalyst bed to a hollow cylinder (a) and of a modified 7 mm Bruker MAS NMR probe equipped with an injection head (b).

Fig. 4 consists of the stator equipped with bearing cartridges at the bottom and top, the reactant gas endcap, the product gas endcap, the rotor, and the driving turbine [18,19]. The bearing and driving cartridges were made by Vespel® and are press-fitted into the housing. The cartridges contain two Si_3N_4 ball bearings and two sets of Vespel® baffles. The baffles are located at both ends of the cartridge, and have to isolate the driving gas from the reactant gas. The rotor is supported by the two ball bearings of the cartridges. The turbine is press-fitted onto the rotor and is located between the the ball bearing at the bottom and the rotor. The rotor is one piece of boron nitride with two distinct parts, a hollow axis and a sample chamber. The reactant gas enters the hollow axis of the turbine part and flows into the sample volume. The large end of the sample volume is press-fitted into the rotor cap. Baffles are located in the endcaps to isolate the product gas and

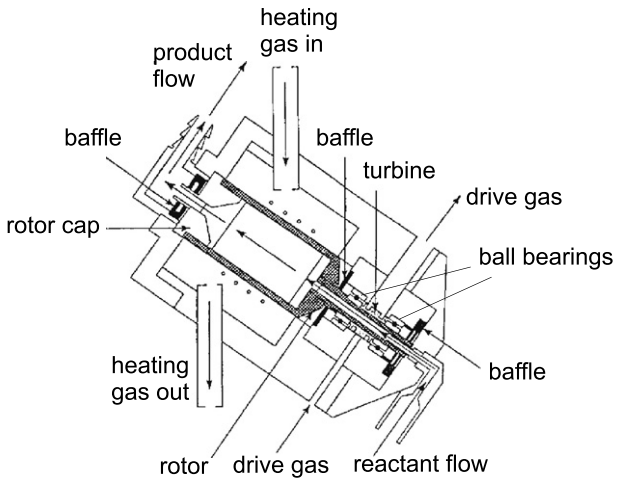


Fig. 4. The upper part of a flow MAS NMR probe with ball bearings and separate gas flows (after Ref. [18]).

the surrounding gas. This mechanical flow MAS NMR probe is suitable for reaction temperatures up to about 600 K and spinning rates of 1–2 kHz [18].

A technique based on the hopping of the flow reactor around an axis at the magic angle was introduced by Maciel and co-workers [20]. The corresponding technique is called GRASSHopper (gas reactor and solid sample hopper). In 1985, the same group developed the principles of magic angle hopping (MAH) [21]. In this experiment, the sample chamber hops by 120° about an axis at the magic angle. Between each jump, the sample chamber is stationary and one NMR experiment is carried out. The hopping is performed by a step motor, which drives a shaft that is coupled via a gear system to the sample chamber (Fig. 5).

After a complete MAH cycle of three orientations, the MAH device is re-initialized by rotating backward to the

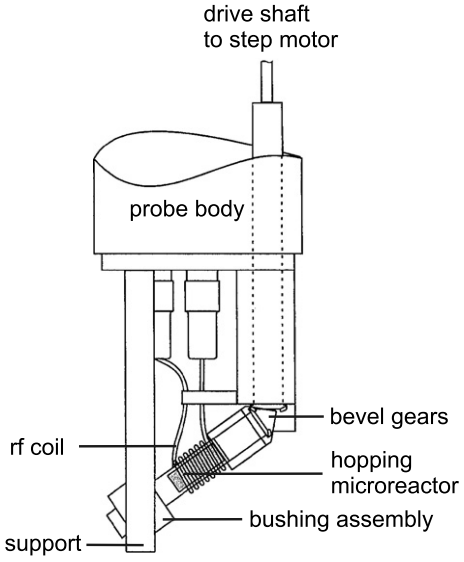


Fig. 5. A flow MAS NMR probe with a hopping microreactor (GRASS Hopper II) [20].

initial orientation. Therefore, flexible and gas-tight input and output lines from the peripheral equipment to the sample chamber of the GRASSHopper device can be used and allow a rotation of the microreactor filled with the working catalyst. In the flow MAH NMR experiments described by Maciel and co-workers [21], the 120° hop time was $t_{hop} = 30$ ms. A requirement of the MAH technique is that t_{hop} is small in comparison with the spin lattice relaxation time T_1 of the resonating nuclei. In addition, the MAH must be accomplished in such a manner that no slippage of the particles in the sample chamber occurs. The experiments were performed with a pulse sequence based on an 8-pulse refocusing cycle [21].

2.2. Peripheral equipment and protocols of flow MAS NMR experiments

In situ flow MAS NMR experiments require conditions similar to those utilized for catalytic investigations with standard fixed-bed reactors [10,11,16]. As an example, Fig. 6 shows the scheme of a gas supply system and the coupling of the flow MAS NMR probe with an on-line analysis equipment for the detection of volatile reaction products. The corresponding analysis equipment could be an on-line gas chromatograph [10,11] or a mass spectrometer [16]. In the case of liquid reactants, the carrier gas 1 (N_2, He, Ar etc.) is loaded with the vapor of this reactant in a thermostated saturator. Carrier gas 1 loaded with reactants is often mixed with gas 2 at the outlet of the saturator. This gas 2 can be a second reactant or a standard gas. The standard gas (neopentane, methane, etc.) is not converted on the catalyst and is utilized as an internal reference for the quantitative evaluation, e.g., of the gas chromatogram of the reaction products.

The flow rates of gases 1 and 2 are controlled by mass flow controllers. To exclude condensation of the reactant vapor inside the tubes connecting the saturator and the flow MAS NMR probe, the temperature of the thermostated saturator should be significantly lower (at least 5 K) than room temperature. The bypass at the saturator allows purging of the catalyst inside the probe with dry carrier gas. The bypass at the flow MAS NMR probe is suitable for testing the reactant flow and the peripheral analysis system without the MAS NMR probe. The outlet of the MAS NMR rotor is not gas-tight and a pump between the probe outlet and the on-line gas chromatograph or mass spectrometer is responsible for maintaining a constant flow of the exhaust gas.

Fig. 7 gives an overview on the different protocols, which are utilized for *in situ* flow MAS NMR experiments [22]. In a continuous-flow experiment (Fig. 7a), the steady state of a heterogeneously catalyzed reaction is investigated. After transferring the calcined catalyst into the MAS NMR probe, the injection of the reactant flow into the rotor is started. The steady state of the heterogeneously catalyzed reaction is often studied at different tempera-

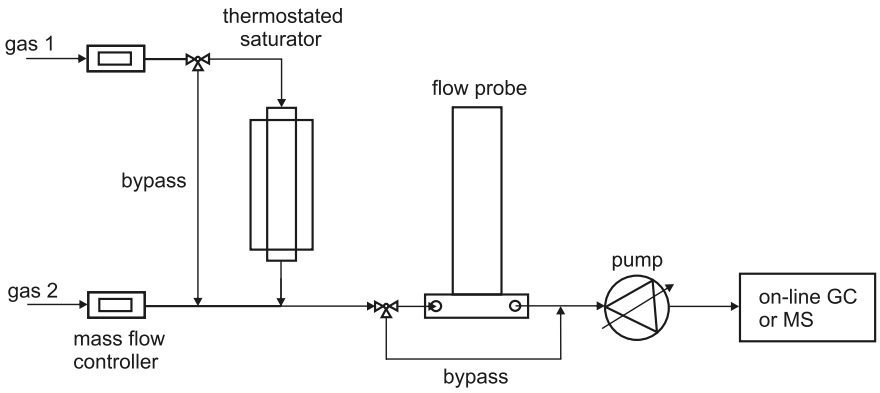


Fig. 6. Scheme of the coupling of a flow MAS NMR probe with mass flow controllers, saturator, and peripheral equipment for the on-line analysis of volatile reaction products (GC: gas chromatograph, MS: mass spectrometer).

tures, as indicated by the temperature profile in Fig. 7a, and with an on-line analysis of volatile reaction products by gas chromatography or mass spectrometry.

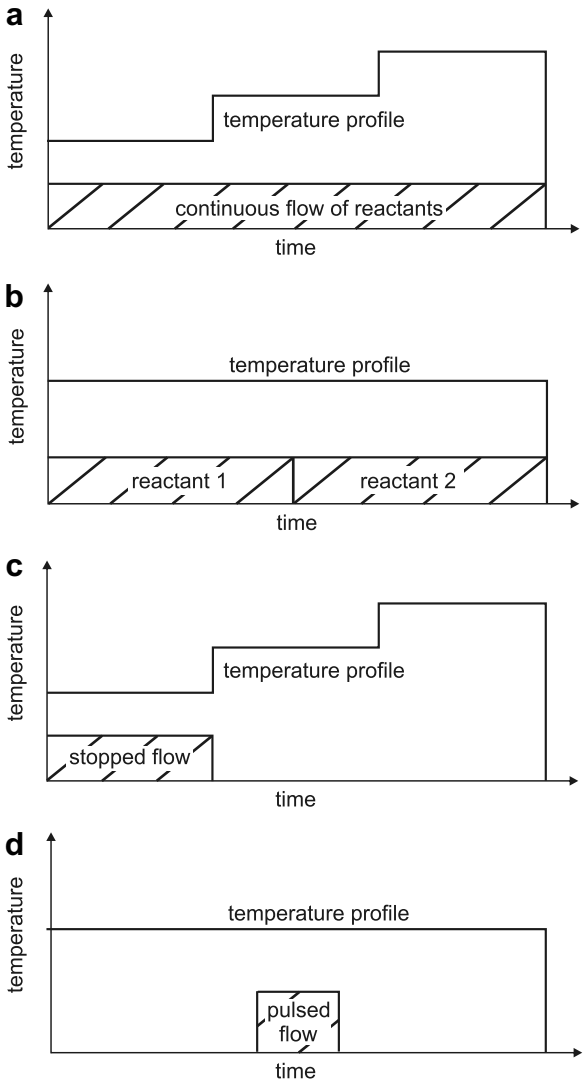


Fig. 7. Time protocols of (a) continuous-flow, (b) switched-flow, (c) stopped-flow, and (d) pulsed-flow experiments (after Refs. [22–24]).

The switched-flow experiment in Fig. 7b corresponds in the first period to the continuous-flow experiment allowing the study of the conversion of reactant 1 at the steady state of the reaction. After a certain time, however, the flow of reactant 1 is stopped and reactant 2 is injected into the MAS NMR rotor. In the second period of the switched-flow experiment, the response of the reaction system on the replacement of reactant 1 by reactant 2 is observed. Reactants 1 and 2 could be, for example, chemically identical compounds, but different in their isotopic enrichment, such as ^{13}C-enriched methanol and non-enriched methanol (see Ref. [23]). In this case the response of the change of ^{13}C-enrichment of the reactants on the isotopic composition of organic deposits formed on the catalyst surface can be investigated [23].

The stopped-flow experiment depicted in Fig. 7c consists of a first period with a continuous conversion of reactants on the catalyst inside the MAS NMR rotor [24]. After a certain reaction time, which leads to the formation of specific intermediates, surface complexes, or deposits, the reactant flow is stopped. Subsequently, the nature of these surface species and their further reaction at elevated temperatures are investigated. Often, the spent catalyst is purged with dry carrier gas after the reactant flow has been stopped and before the MAS NMR spectroscopic studies are started. During this purging period, non-converted reactants and volatile reaction products are removed. Otherwise, the signals of these residual reactants and reaction products would superpose on the signals of surface compounds under study and they could complicate the study of the chemical conversion of these surface compounds.

In the pulsed-flow experiment shown in Fig. 7d, the catalyst sample inside the MAS NMR rotor is heated at elevated and constant temperature and, for a short duration, a pulse of liquid or gaseous reactants is injected into the MAS NMR rotor. Subsequently, the catalytic conversion or the isotopic exchange of the reactants on the solid catalyst is investigated as a function of time. The pulsed-flow experiment is used for time-resolved investigations of rapid reactions of the injected compounds.

Generally, the chemical conversion of reactants must be in the time scale of NMR spectroscopy for allowing a time-resolved detection by this method. ^{1}H nuclei have typical spin lattice relaxation times of 500 ms to 10 s and require 1–100 scans per spectrum. Therefore, the time scale of ^{1}H MAS NMR spectroscopy combined with a pulsed-flow experiment is of the order of seconds to minutes. In the case of ^{13}C MAS NMR spectroscopy, a time scale of up to several hours must be expected due to spin lattice relaxation times of 1–30 s and a much higher number of scans.

Another situation occurs for MAS NMR studies of heterogeneously catalyzed reactions under continuous-flow conditions. In this case, the life time of intermediates and product molecules on the catalyst surface is the limiting factor in comparison with the duration of the free induction decay. The free induction decay of ^{13}C MAS NMR signals with a line width of ca. 100 Hz has the duration of few milliseconds. This is the lower limit for the life time of intermediates and product molecules, which can be detected by MAS NMR spectroscopy under continuous-flow conditions. In the steady state of a reaction under flow conditions, a continuous formation of intermediates and product molecules occurs. At each scan, therefore, a similar number of intermediates and product molecules exist on the catalyst. In the case of switched-flow and stopped-flow experiments, organic deposits with a long life time on solid catalysts are often studied, which do not limit the application of *in situ* MAS NMR spectroscopy.

A serious problem of continuous-flow experiments, however, can be the short residence time of reactants in the magnetic field before performing the NMR experiment. In order to reach the full Boltzmann distribution, the molecules injected into the MAS NMR rotor must reside longer than 5 times the spin lattice relaxation time T_1 inside the magnetic field. Generally, the equilibrium magnetization is reached in the magnetization volume, V_{mag}, which is the volume of the sample plus that of the tubes of the flow MAS NMR probe inside the magnetic field B_0. In some cases, a pre-magnetization in a second external magnetic field is performed. To reach the full Boltzmann distribution of the flowing reactant molecules applied in a continuous-flow experiment, the maximum flow rate, F_{max}, is [25]:

$$F_{max} = \frac{V_{mag}}{5T_1}. \quad (1)$$

For a typical magnetization volume V_{mag} of a flow MAS NMR probe of ca. 1.5 ml and a spin lattice relaxation time of the nuclear spins under study of ca. 10 s, Eq. (1) leads to the maximum flow rate of 30 μl/s corresponding to 1.8 ml/min. This flow rate is valid for the empty sample volume. In the case of heterogeneous catalysis on mesoporous and microporous solids, the residence time of reactant molecules adsorbed at the active surface sites inside the pore system of catalyst particle, however, is much longer than in an empty sample volume. This leads to a significantly longer residence time of the reactant molecules in the rotor and a higher magnetization. In this case, much higher flow rates of reactant molecules than obtained by Eq. (1) can be applied for MAS NMR experiments under continuous-flow conditions. However, for each reaction system (combination of reactants and porous catalyst) the influence of the reactant flow rate on the magnetization of these reactants should be considered and tested.

2.3. MAS NMR-UV/Vis technique

A very recent development is the combination of *in situ* MAS NMR spectroscopy with another spectroscopic method, such as *in situ* UV/Vis spectroscopy, in a single probe. For applications in the field of heterogeneous catalysis, this technique is suitable, for example, for simultaneous MAS NMR and UV/Vis studies of the formation of polyenic and aromatic compounds and carbenium ions on the surface of solid catalysts [26].

The probe used for MAS NMR-UV/Vis spectroscopy is based on those in Figs. 1–3. As shown in Fig. 8, a glass fiber is attached to the bottom of the stator. In addition, the MAS NMR rotor is equipped at the bottom with a quartz window. Via the quartz window and the glass fiber, the catalyst material in the sample volume of the MAS NMR rotor can be investigated by a fiber optic UV/Vis spectrometer. This MAS NMR-UV/Vis probe is suitable for experiments under continuous-flow condition [26] as well as under batch conditions [27]. In the latter case, the probe is used without an injection tube.

For the MAS NMR-UV/Vis studies described in Refs. [26–28], 7 mm Bruker and 7 mm Doty MAS NMR probes were modified according to Fig. 8. In the case of the Bruker MAS NMR probe, 7 mm MAS NMR rotors of probes with a Laser-heating system were equipped at the bottom with a quartz glass window (Hellma GmbH & Co. KG, Müllheim, Germany) instead of the sample insert. This MAS NMR rotor, which is shown in Fig. 3a, was used in a variable-temperature 7 mm Bruker MAS NMR probe with an air heating system. At the bottom of the 7 mm Bruker MAS NMR sta-

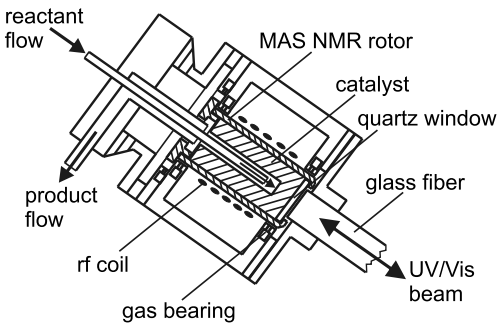


Fig. 8. A flow MAS NMR probe, which is equipped with a glass fiber for UV/Vis spectroscopy in reflection mode [26].

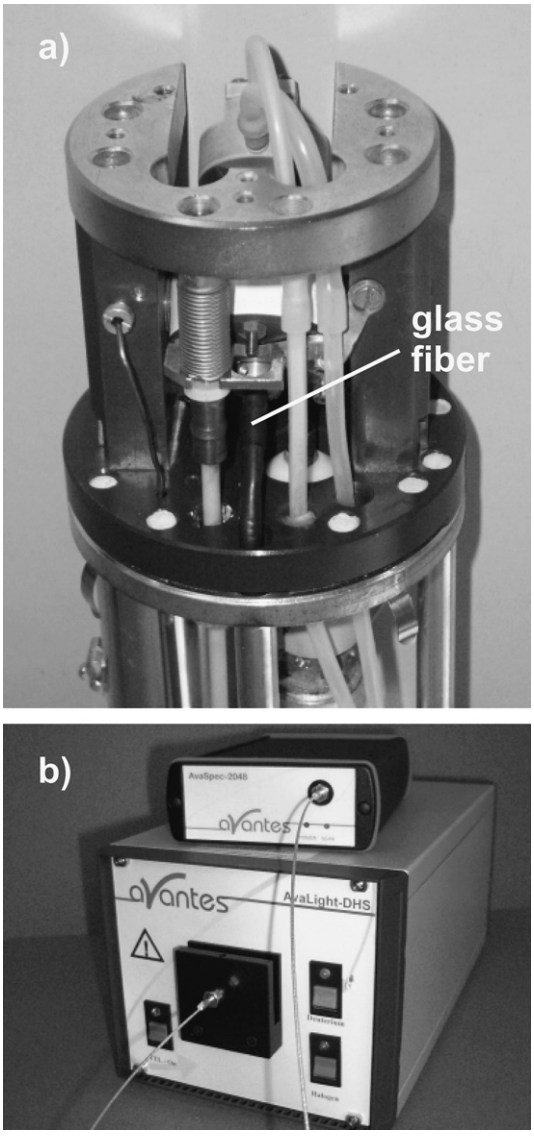


Fig. 9. (a) A modified 7 mm Bruker MAS NMR probe equipped with a glass fiber for UV/Vis spectroscopy and (b) the corresponding UV/Vis light source and UV/Vis spectrometer.

tor, a support for fixing the glass fiber was added (Fig. 9a). UV/Vis spectra are recorded, e.g., with an AvaLight-DH-S deuterium light source, an AvaSpec-2048 fiber optic spectrometer, and a glass fiber reflection probe FCR-7UV20-3-SR-S1 of Avantes Inc., CO, USA (Fig. 9b). This UV/Vis equipment allows investigations in the spectral range of 200–800 nm.

In the case of the 7 mm high-temperature Doty MAS NMR probe of type DSI-740, Doty Scientific Inc., Columbia, USA, a modified sample insert for the MAS NMR rotors with a quartz glass window at the bottom is used. A support was added at the bottom of the stator to fix the glass fiber optics. The modified 7 mm Doty MAS NMR probe is suitable for MAS NMR-UV/Vis investigations at temperatures of up to 723 K and sample spinning rates of up to 3 kHz.

2.4. Application of hyperpolarized xenon in flow MAS NMR spectroscopy

To improve the sensitivity of NMR spectroscopy, the application of hyperpolarized xenon has been investigated and utilized by a number of groups [15,29–33]. The principle of this technique consists of an optical pumping of rubidium vapor at the wavelength of the D1 transition of rubidium (794.8 nm) with circularly polarized light of a laser, e.g., a 60 W diode array laser [15]. In the equipment shown in Fig. 10, a gas mixture with a pressure of ca. 2 bar containing approximately 1% natural abundance xenon and 99% helium is purified in an oxygen trap and leads to the optical pump cell made of Pyrex. Spin exchange occurs between the excited rubidium atoms and the xenon atoms by gas phase collisions. This spin exchange results in xenon atoms with a non-equilibrium nuclear spin polarization of 5–8% (hyperpolarization). After passing through a rubidium trap and a needle valve, the hyperpolarized xenon is injected with a pressure of about 1 bar into the sample volume of the flow MAS NMR probe. PFA (perfluoralkoxy copolymer) plastic needle valves and tubes minimize the loss of polarization via xenon-wall relaxation.

A direct study of hyperpolarized xenon adsorbed in the pore system of solid catalysts can be performed by ^{129}Xe flow MAS NMR spectroscopy [15,29]. In some cases, a second polarization transfer between the hyperpolarized xenon and atoms on the surface of solid catalysts is carried out via the nuclear Overhauser effect. Applications and details of this technique, e.g., for a selective enhancement of the NMR signals of surface OH groups on solid catalysts and adsorbents are described in Refs. [30–33].

2.5. Temperature behavior of in situ MAS NMR probes

The study of heterogeneously catalyzed reactions at elevated temperatures inside a solid-state NMR probe, i.e., under *in situ* conditions, requires an accurate determination of the absolute temperature and the temperature gradient over the sample volume of the probe. As described by Sundaramurthy et al. [16], there is often a systematic error in the temperature displayed by the thermocouple acting as temperature sensor in the probe. Methods for the temperature calibration of the solid-state NMR probes under working conditions and for the study of the temperature gradient over the sample volume are important prerequisites for reproducible *in situ* MAS NMR investigations of heterogeneously catalyzed reactions.

A suitable method for determining the temperature, T, inside the sample volume of a solid-state NMR probe is the quantitative evaluation of the absolute NMR signal intensity using Curie's law [34]. According to Curie's law, the signal intensity is directly related to $1/T$. However, this approach is limited to heating systems, which heat the sample volume only, such as Laser heating systems, and not the radio frequency coil or other electronic parts of the probe. Heating of the radio frequency coil strongly affects the

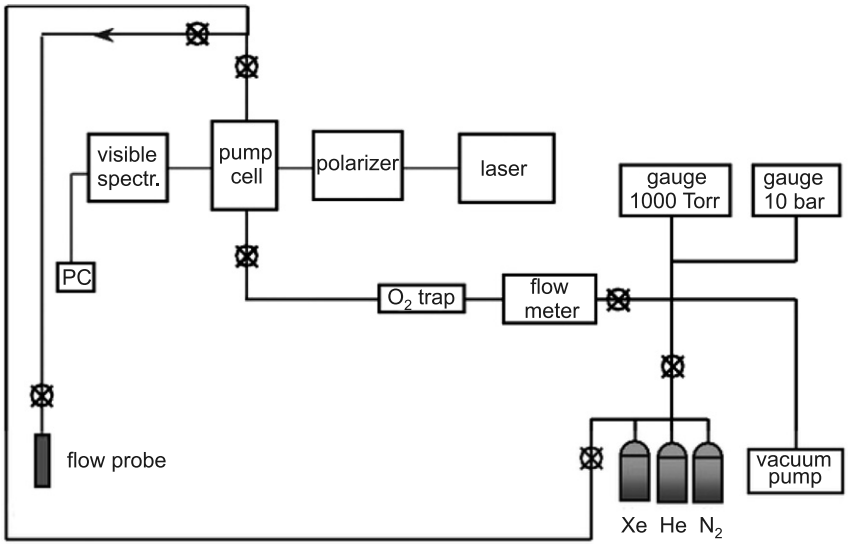


Fig. 10. Continuous-flow system for the production of hyperpolarized xenon and the injection of xenon into a flow MAS NMR probe [15].

quality factor of the NMR probe and causes a change of the signal intensity, which is then very different from that predicted by Curie's law.

A very accurate and often utilized method for calibrating the temperature behavior of *in situ* solid-state NMR probes is the study of melting points and phase transitions (Table 1). An additional way consists of the investigation of materials with temperature-dependent chemical shifts (a shift thermometer). Often, both these methods are combined allowing a temperature calibration with high accuracy over a broad temperature range.

Starting with the calibration by melting points and phase transitions, different shift thermometers were developed for solid-state NMR spectroscopy. Wehrle et al. [41] investigated the line splitting in the ^{15}N CPMAS NMR spectrum of the organic dye molecule tetramethyldibenzotetraaza annulene (TTAA) in the temperature range of $T = 123$–405 K. Pan and Gerstein [42] found the following temperature dependence of the ^{31}P NMR shift of paramagnetic $(VO)_2P_2O_7$ in the temperature range of $T = 285$–353 K.

$$\delta = 414.621/T + 1118.4 \quad (2)$$

The most often used chemical shift thermometer is the ^{207}Pb resonance of $Pb(NO_3)_2$. However, different authors published different slopes of 1.22 K/ppm [16], 1.29 K/ppm [43], and 1.33 K/ppm [35], which may be due to the different temperature ranges investigated. Studying the ^{207}Pb NMR shift of $Pb(NO_3)_2$ in the temperature range of $T = 303$–673 K, the following expression was found [38]:

$$T = -5.2 \times 10^{-4}\delta^2 + 1.3\delta + 30.1 \quad (3)$$

Utilizing $Pb(NO_3)_2$ as a shift thermometer, Sundaramurthy et al. [16] demonstrated that the injection of flowing nitrogen (50 ml/min) into a flow MAS NMR probe at 473 K leads to a temperature decrease of just 2 K. Furthermore. Eq. (3) can be used to determine the temperature gradient, ΔT, of variable-temperature MAS NMR probes under working conditions [44]. The ^{207}Pb MAS NMR spectra of $Pb(NO_3)_2$ shown in Fig. 11 were recorded with a modified 7 mm Doty MAS NMR probe during injection of the nitrogen flow of 15 ml/min. These experiments indicate that a negligible increase of the temperature gradient of only ca. 1 K occurs upon heating from 373 to 673 K.

Table 1
Melting points and phase-transition temperatures of various materials used for the calibration of NMR probes at elevated temperatures

Compound	Melting point (K)	Phase transition temperature (K)	References
Benzene	279		[35]
2,2-Dimethylpropane-1,3-diol		315	[36]
carbon tetrabromide		320	[37]
4-Cyano-4′-7-alkoxybiphenyls	347	327	[38]
Samarium acetate tetrahydrate		343	[39]
1,4-Diazabicyclo-[2,2,2]-octane (DABCO)		351	[37,40]
Benzoic acid	395		[16]
4-Cyano-4″-5-terphenyl		404	[38]
Adipic acid	425		[16]
Citric acid	426		[35,38]
Rubidium nitrate		447	[37]
Sodium nitrate	580		[38]
Lithium iodide	742		[38]
Lithium sodium sulfate		791	[37]

3. ^{129}Xe MAS NMR spectroscopic investigations of the pore system of solid catalysts using hyperpolarized xenon under continuous-flow conditions

3.1. Studies of the pore architecture of ITQ-6

Adsorption of xenon atoms as probes for studying porous adsorbents and catalysts gives unrivalled information about the pore architecture of these materials. This is due to the dependence of the chemical shift of ^{129}Xe nuclei interpolated to a xenon pressure of zero on the pore sizes of the solid materials under study [45–48]. The optical

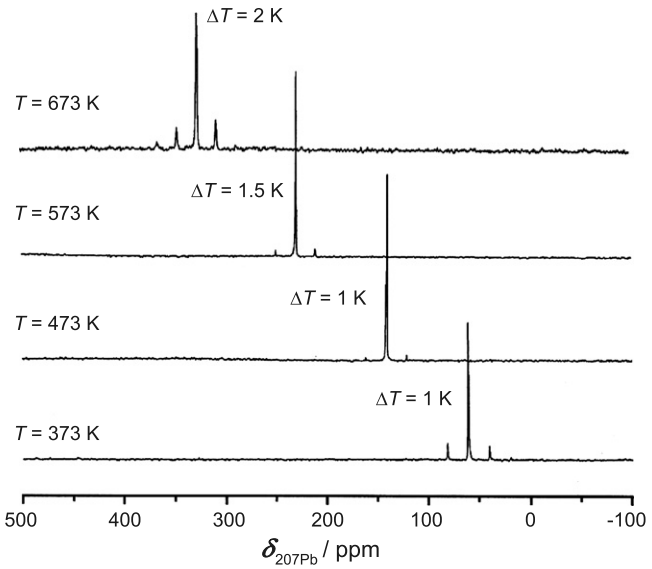


Fig. 11. ^{207}Pb MAS NMR spectra of $Pb(NO_3)_2$ recorded during injection of 15 ml nitrogen per minute in a 7 mm flow Doty MAS NMR probe. The parameter ΔT is the experimentally derived temperature gradient over the sample volume. The experiments were performed in a magnetic field of $B_0 = 9.4$ T, at the resonance frequency of 83.5 MHz, with the sample spinning rate of $\nu_{rot} = 1.8$ kHz, the repetition time of 5 s, and ca. 100 scans per spectrum [44].

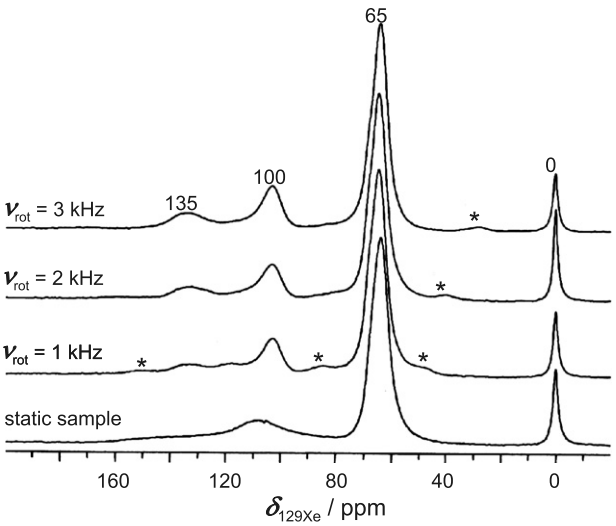


Fig. 12. Solid-state ^{129}Xe NMR spectra of zeolite ITQ-6 recorded under a flow of 100 ml/min of a 1% hyperpolarized xenon and sample spinning rates of 0 kHz (static sample) to 3 kHz. The experiments were performed in a magnetic field of $B_0 = 7.0$ T, at the resonance frequency of 83.0 MHz, with the repetition time of 1 s, and 1024 scans per spectrum [15].

pumping of xenon for producing hyperpolarized nuclear spins leads to a strong increase of the sensitivity of this method. The optically enhanced polarization is 4–6 orders of magnitude higher than the thermal polarization [15]. The technique utilized for the formation of hyperpolarized xenon is described in Section 2.4. In a number of investigations, the advantages of hyperpolarized xenon for studies of porous solids, such as of zeolites [15], mesoporous films [49], and multicomponent porous materials [50] have been demonstrated.

An example of the application of hyperpolarized xenon in combination with the flow MAS NMR technique is the study of ITQ-6, i.e., of a material, which was prepared by delamination of layered precursors of ferrierite (FER-type zeolite) [15]. The delamination was performed by placing the slurry of the layered zeolite precursors in an ultrasound bath. The resulting material consists of irregularly oriented monolayers of FER-type zeolite with void space between the layers [51]. Ferrierite consists of small cages, where only a single xenon atom can enter, and a two-dimensional channel system with 8- and 10-membered oxygen rings [52]. In the channels, xenon can be packed so that xenon–xenon interactions occur.

Fig. 12 shows solid-state ^{129}Xe NMR spectra of zeolite ITQ-6 recorded under a flow of hyperpolarized xenon without sample spinning (bottom) and with sample spinning rates of 1–3 kHz (top) [15]. The signal at 65 ppm, which is not observed for highly crystalline ferrierite, is caused by xenon in the inter-lamellar space. The two signals at 100 and 135 ppm correspond to xenon adsorbed in small cages and in channels, respectively. In comparison with solid-state ^{129}Xe NMR spectra of hyperpolarized xenon adsorbed on highly crystalline ferrierite, the spectra of ITQ-6 show a significantly weaker signal at 135 ppm. This finding indicates that the delamination of the zeolite lattice proceeds along the channels [15]. The comparison of the spectra recorded without and with MAS techniques demonstrates that sample spinning is required for reaching a suitable spectral resolution.

By the use of the laser-polarization equipment depicted in Fig. 10 combined with a flow MAS NMR probe, the xenon polarization can be restored after each NMR experiment. In this way, ^{129}Xe 2D-exchange MAS NMR experiments are possible within a reasonable measurement time. Generally, 2D-exchange NMR experiments monitor changes in resonance frequencies occurring on a time scale ranging from milliseconds to few seconds. This is reached by monitoring the resonance frequencies before and after the mixing time, t_m, during which spin exchange can occur. These frequency changes are manifested by off-diagonal peaks in the 2D-exchange NMR spectrum, which depend on the duration of the mixing time [53].

The ^{129}Xe 2D-exchange MAS NMR spectrum of ITQ-6 obtained with mixing times of $t_m = 1$ ms and shorter consisted of diagonal peaks at 65, 110, and 135 ppm, but no cross peaks occurred (not shown) [15]. However, with longer mixing times, such as $t_m = 50$ ms (Fig. 13), cross peaks appear, which indicate that exchange takes place between the gas phase and the inter-lamellar space (a), between cavities and the inter-lamellar space (b), and between xenon in the channels and cavities (c). If the shapes of the diagonal peaks in Fig. 13 are considered, the peak for xenon adsorbed in the channels (135 ppm) is strongly elongated along the diagonal, while the diagonal peak of xenon in the cavities (100 ppm) has a symmetric shape. The elongated line shape results from a distribution of slightly different adsorption sites in the channels. In addition, it indicates that during the mixing time

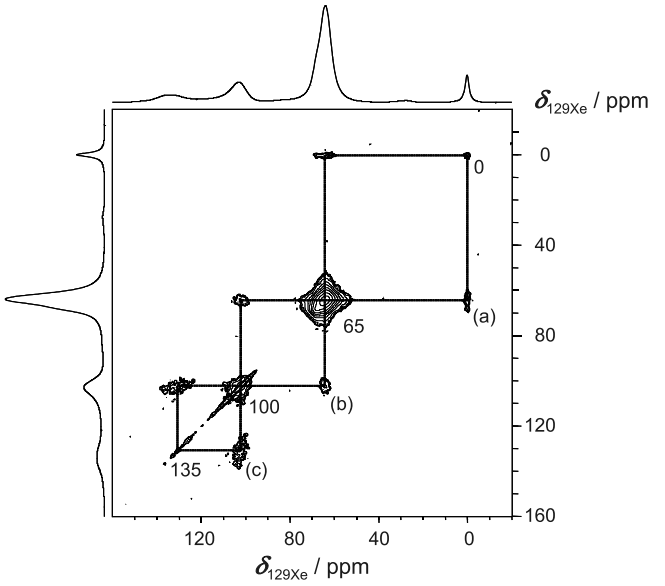


Fig. 13. ^{129}Xe 2D-exchange MAS NMR spectrum of zeolite ITQ-6 recorded under a flow of hyperpolarized xenon and with a mixing time of $t_m = 50$ ms. The experiments were performed in a magnetic field of $B_0 = 7.0$ T, at the resonance frequency of 83.0 MHz, with the sample spinning rate of $\nu_{rot} = 3$ kHz, with the repetition time of 2 s, and 8 scans per spectrum [15]. The assignments (a), (b), and (c) of the diagonal peaks are given in the text.

there is no direct exchange of xenon between different channels. However, exchange of xenon between the channels and the cavities occurs.

3.2. Real time studies of adsorption processes on porous catalysts

Due to the high sensitivity of ^{129}Xe MAS NMR spectroscopy with hyperpolarizedxenon, the flow MAS NMR technique can be utilized to study modifications of the void space in porous solids in real time, such as caused by adsorption and diffusion of reactant molecules. As an example, Fig. 14 shows MAS NMR spectra of hyperpolarized xenon (1% xenon in helium) on silicalite-1 recorded before and after adsorption of benzene under flow conditions [28]. Before benzene is adsorbed on silicalite-1, the ^{129}Xe MAS NMR spectrum consists of a weak signal at 0 ppm caused by gaseous xenon and a strong signal at 103 ppm due to xenon adsorbed in the empty channels of silicalite-1 (Fig. 14a). Upon short exposure of the sample to a flow of 1.3% benzene vapor in helium, the narrow signal at 103 ppm is replaced by a broad one at 123.8 ppm (Fig. 14b). This change of the resonance position is explained by the presence of benzene molecules in the channels of silicalite-1, which causes a decrease of the effective pore diameter. After stopping the benzene flow, the chemical shift and line width of the broad low-field signal is decreased with time (Fig. 14c). Hence, desorption of benzenes molecules under flowing helium occurs. Further benzene pulses result in characteristic changes of the ^{129}Xe MAS NMR spectra (Fig. 14d–f), equal to those in Fig. 14b and c. As demonstrated for adsorption of benzene on silicalite-1, ^{129}Xe MAS NMR spectroscopy of hyperpolarized xenon under flow conditions can be utilized for the investigation of the location of reactant and adsorbate molecules in the cages and pores of catalysts and a variety of other porous solids.

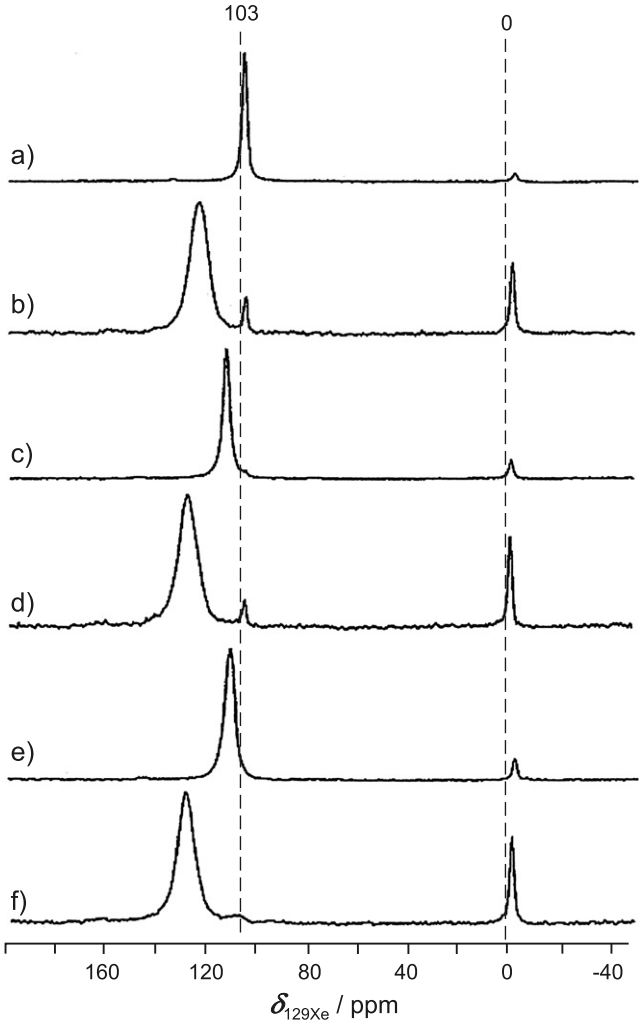


Fig. 14. Evolution of the ^{129}Xe MAS NMR spectra of silicalite-1 recorded during a flow of hyperpolarized xenon and upon adsorption and desorption of benzene: (a) hyperpolarized xenon on fresh silicalite-1; (b) after a pulse of benzene (ca. 2×10^{20} molecules); (c) 1.5 h later; (d) after second pulse of benzene (ca. 2×10^{20} molecules); (e) 1.5 h later; (f) after third pulse of benzene (ca. 2×10^{20} molecules). The experiments were performed in a magnetic field of $B_0 = 7.0$ T, at the resonance frequency of 83.0 MHz, and with the sample spinning rate of $\nu_{rot} \cong 3.5$ kHz [29].

4. Studies of the behavior of solid catalysts and of reaction mechanisms in heterogeneous catalysis by flow MAS NMR spectroscopy

4.1. Coordination change of zeolitic framework atoms upon continuous hydration and dehydration

Microporous silicoaluminophosphates (SAPO's) are of increasing interest for applications as solid acids in heterogeneous catalysis. Replacement of phosphorus atoms at

tetrahedral sites by silicon atoms in the aluminophosphate framework (P → Si) leads to the formation of ≡Si–O–Al≡ bridges. In this case, the negative charges formed at the tetrahedrally coordinated framework aluminum atoms are not balanced by an equal number of positively charged phosphorus atoms and must be compensated by hydroxyl protons of bridging OH groups (SiOHAl) [54]. Therefore, incorporation of silicon atoms into the framework of aluminophosphates leads to the formation of Brønsted acid sites making the silicoaluminophosphates interesting materials for acid catalyzed reactions [55–57]. However, a loss of crystallinity upon rehydration of calcined silicoaluminophosphates was found [58,59], which could be a limitation for the application of these catalysts in industrial processes and required, therefore, a detailed study of this effect.

One of the most interesting silicoaluminophosphates, e.g., for the conversion of methanol to olefins (MTO process), is H-SAPO-34 [12]. The hydration- and dehydration-induced changes of the framework of H-SAPO-34 has been studied by *in situ* ^{1}H and ^{27}Al MAS NMR spectroscopy during continuous adsorption and desorption of water. The behavior of surface sites and the coordination of aluminum atoms in the silicoaluminophosphate framework were monitored during the continuous injection (25–50 ml/min) of nitrogen loaded with water vapor (hydration) or of dry nitrogen (dehydration) into a 4 mm flow MAS NMR probe [12].

Fig. 15 shows ^{1}H and ^{27}Al MAS NMR spectra recorded during the continuous hydration of calcined H-SAPO-34. The ^{1}H MAS NMR spectrum of the calcined material recorded before starting the hydration is dominated by the signal of bridging OH groups (SiOHAl) at 3.4 ppm and a weak high-field shoulder (ca. 2 ppm) due to a small number of defect SiOH groups (Fig. 15a, left). The ^{27}Al MAS NMR spectrum consists of a strong signal at 34 ppm due to tetrahedrally coordinated framework aluminum atoms (Fig. 15a, right). The weak high-field shoulder at ca. 8 ppm is caused by a small number of pentacoordinated aluminum atoms [12].

Upon adsorption of 0.8–1.3 mmol/g water molecules, a significant decrease of the ^{1}H MAS NMR signal of SiOHAl groups at ca. 3.4 ppm occurs accompanied by the appearance of a broad signal at ca. 5.2 ppm due to water molecules (Fig. 15b and c). The resonance position of this water signal indicates the presence of hydrogen bonded water molecules and the formation of hydroxonium ions, which are involved in a rapid chemical exchange [60,61]. A change in the ^{27}Al MAS NMR signals is not found until a water adsorption of ca. 5 mmol/g. According to this observation, the hydration of calcined H-SAPO-34 starts with an adsorption of water molecules exclusively at SiOHAl groups up to a coverage of approximately three water molecules per hydroxyl group.

The ^{1}H MAS NMR spectra of H-SAPO-34 loaded with 10.5 mmol/g water molecules and more (Fig. 15d and e, left) are dominated by a broad signal of bulk water at ca. 4.8 ppm. In the ^{27}Al MAS NMR spectra, the occurrence

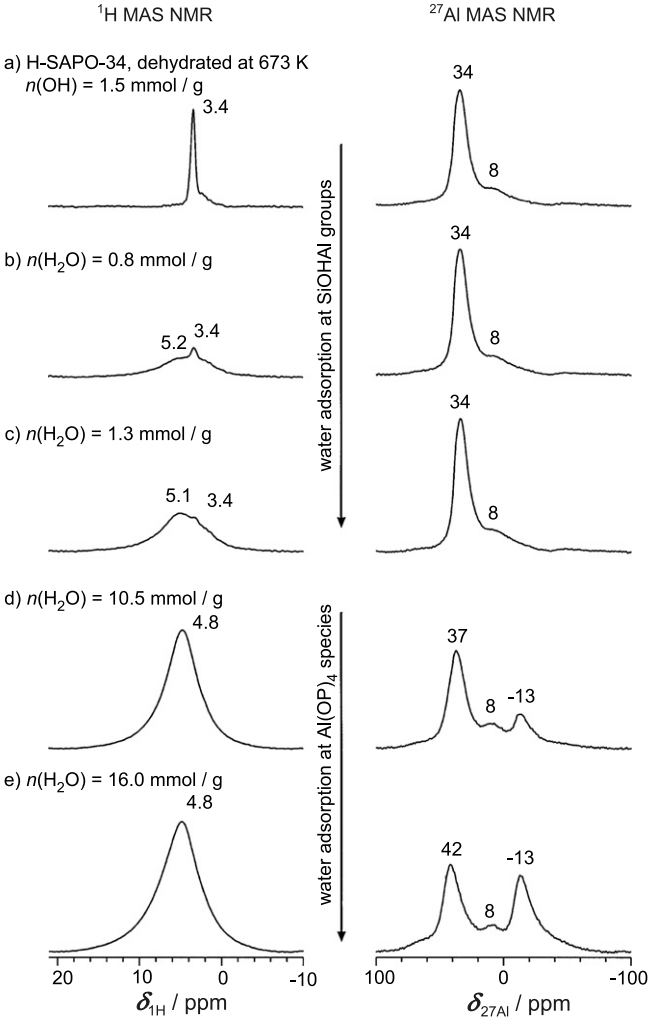


Fig. 15. ^{1}H (left) and ^{27}Al MAS NMR spectra (right) of the silicoaluminophosphate H-SAPO-34 recorded at $T = 298$ K during continuous hydration of the calcined sample using a flow of nitrogen loaded with water vapor. The numbers of adsorbed water molecules (left-hand side) were determined by the quantitative evaluation of the ^{1}H MAS NMR spectra. The experiments were performed in a magnetic field of $B_0 = 9.4$ T, at resonance frequencies of 400.1 and 104.3 MHz, with repetition times of 10 s and 500 ms and 64 and 1200 scans per spectrum, respectively, and with the sample spinning rate of $\nu_{rot} = 10$ kHz [12].

of a weak signal at −13 ppm indicates the formation of octahedrally coordinated aluminum atoms via coordination of water molecules to aluminum atoms in ≡P–O–Al≡ bridges (Fig. 15d and e, right). A significant increase of the ^{1}H MAS NMR signal of defect SiOH groups at ca. 2 ppm is not found neither for weakly hydrated H-SAPO-34 nor for strongly hydrated H-SAPO-34. This indicates that the adsorption of water molecules on H-SAPO-34 does not lead to a breakage of ≡Si–O–Al≡ bridges in the framework.

^{1}H and ^{27}Al MAS NMR investigations of the dehydration of H-SAPO-34 under dry nitrogen flow indicated that this process is also characterized by two steps [12]. Desorption of water molecules coordinated to aluminum atoms in ≡P–O–Al≡ bridges already occurs at 298 K (Fig. 16a–c).

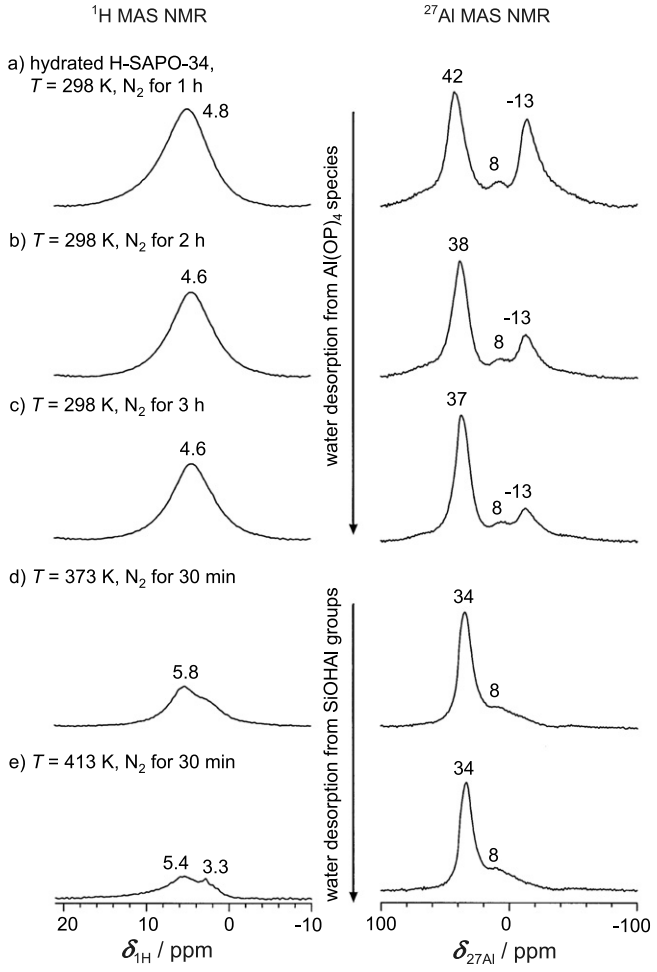


Fig. 16. ^{1}H (left) and ^{27}Al MAS NMR spectra (right) of hydrated silicoaluminophosphate H-SAPO-34 recorded at $T = 298$–413 K during continuous dehydration in a flow of dry nitrogen. The numbers of adsorbed water molecules (left-hand side) were determined by the quantitative evaluation of the ^{1}H MAS NMR spectra. The experiments were performed in a magnetic field of $B_0 = 9.4$ T, at resonance frequencies of 400.1 and 104.3 MHz, with repetition times of 10 s and 500 ms and 64 and 1200 scans per spectrum, respectively, and with the sample spinning rate of $\nu_{rot} = 10$ kHz [12].

The intensity of the ^{27}Al MAS NMR signal of octahedrally coordinated aluminum atom at −13 ppm decreases, while the signal of tetrahedrally coordinated aluminum atoms at 37–42 ppm increases. Hence, the hydration of ≡P–O–Al≡ bridges in the framework of H-SAPO-34 is a reversible process on the time scale of solid-state NMR experiments. The second dehydration step, i.e., the dehydration of SiOHAl groups, requires temperatures of at least 373 K (Fig. 16d and e). Again, ^{1}H MAS NMR spectroscopy shows that there is no breakage of ≡Si–O–Al≡ bridges and formation of defect SiOH groups.

^{1}H and ^{27}Al MAS NMR spectroscopy under continuous-flow conditions has also been applied to the investigation of the ammoniation and deammoniation of silicoaluminophosphates [13]. As in the case of the hydration and dehydration of H-SAPO-34, the ammoniation and deammoniation of this silicoaluminophosphate are two-step processes. The first ammoniation step consists of an adsorption of ammonia exclusively at SiOHAl groups, while the second ammoniation step leads to a coordination of ammonia molecules to framework aluminum atoms in ≡P–O–Al≡ bridges. While the first step is chemisorption of ammonia molecules at acidic OH groups leading to the formation of ammonium ions, the second step is weak physisorption of ammonia accompanied by transformation of tetrahedrally coordinated framework aluminum atoms to octahedrally coordinated aluminum species [13].

4.2. Hydrogenation of toluene on Pt/ZrO_2–SO_4

Bifunctional catalysts are characterized by the presence of Brønsted acid sites and dehydrogenation/hydrogenation centers, which are formed, for example, by highly dispersed platinum or palladium particles. Examples of the application of these catalysts in heterogeneous catalysis are the hydrogenation of olefins and aromatics, the dehydrogenation of alkanes and alcohols, and the skeletal isomerization of alkanes [62]. Sundaramurthy et al. [16] have utilized the flow MAS NMR technique for studying the hydrogenation of toluene to methylcyclohexane on platinum-modified sulfated zirconia (Pt/ZrO_2–SO_4). The catalyst loaded with 0.3% platinum was prepared according to Ref. [63]. The flow MAS NMR equipment utilized for the studies was similar to those shown in Figs. 2 and 6. The activation of the catalyst was performed inside the MAS NMR rotor by heating to 423 K under a nitrogen flow of 43 ml/min. Subsequently, the catalyst was exposed to a flow of hydrogen (40 ml/min) at 423 K for 2 h.

In the first step, ^{1}H MAS NMR spectra of Pt/ZrO_2–SO_4 upon adsorption of pure toluene and pure methylcyclohexane (without hydrogen) under nitrogen flow and at temperatures of 333–423 K were recorded (not shown). These studies allowed the assignment of ^{1}H MAS NMR signals at 2.12–2.61 ppm and 6.99–7.63 ppm to toluene, while signals at 0.95–1.01 ppm, 1.35–1.42 ppm, and 1.76–1.8 ppm were found to be caused by methylcyclohexane [16]. In the second step, toluene hydrogenation on Pt/ZrO_2–SO_4 under continuous-flow conditions was performed using hydrogen as carrier gas loaded with toluene. In addition, hydrogen also plays the role of a reactant.

In Fig. 17, the ^{1}H MAS NMR spectra recorded during the hydrogenation of toluene on Pt/ZrO_2–SO_4 at temperatures of 333–423 K are shown [16]. The chemical shifts of the signals of toluene (tol) and of methylcyclohexane (mch) correspond to those observed upon adsorption of the pure reactants, i.e., without hydrogen. It was found that the spectra are fully reversible. The signals of methylcyclohexane increase upon raising the reaction temperature and those of toluene increase after lowering the temperature. No signals of non-volatile deposits occur in the spectra. The exhaust gas leaving the flow MAS NMR probe, i.e., the reaction products, were simultaneously analyzed by mass spectrometry. In agreement with the results of flow MAS NMR spectroscopy, the mass spectrum obtained at

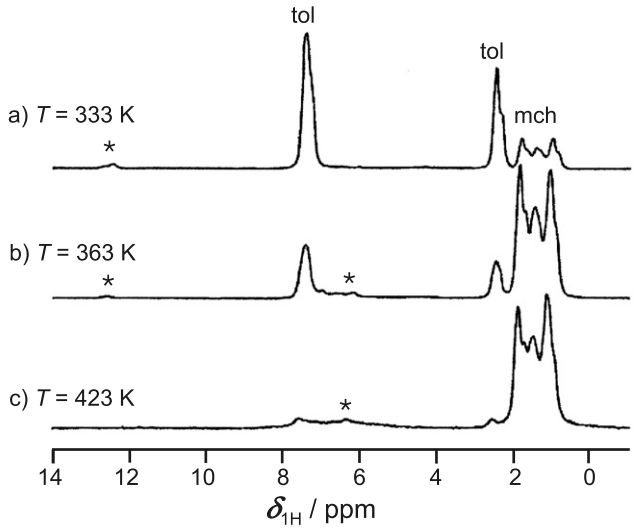


Fig. 17. ^{1}H MAS NMR spectra of Pt-loaded sulfated zirconia (Pt/ZrO_2-SO_4) recorded during toluene hydrogenation under a continuous flow of hydrogen at 333, 363, and 423 K (a, b, and c, respectively). The signals assigned by 'tol' and 'mch' are due to toluene and methylcyclohexane, respectively. The asterisks denote spinning sidebands. The experiments were performed in a magnetic field of $B_0 = 9.4$ T, at the resonance frequency of 400.1 MHz, with the repetition time of 10 s, 16 scans per spectrum, and the sample spinning rate of $\nu_{rot} = 2.1$ kHz [16].

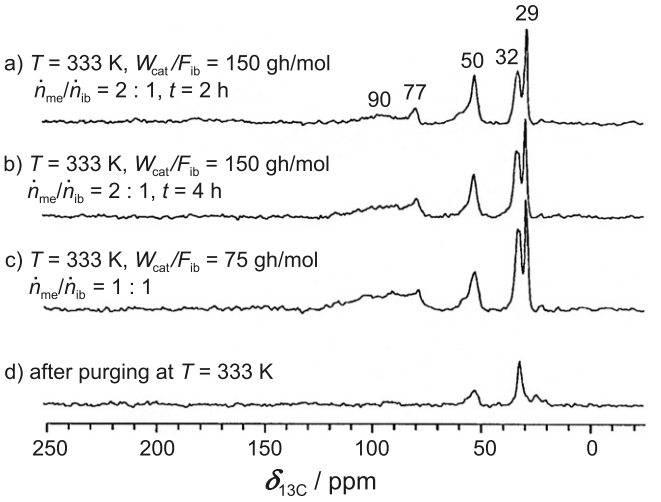


Fig. 18. ^{13}C MAS NMR spectra of zeolite H-Beta recorded during the synthesis of methyl-*tert*-butylether by conversion of isobutene and methanol under continuous-flow conditions (a–c) and after purging the catalyst at 333 K (d). The experiments were performed with high-power proton decoupling in a magnetic field of $B_0 = 9.4$ T, at the resonance frequency of 100.6 MHz, with the repetition time of 10 s, 720 scans per spectrum, and the sample spinning rate of $\nu_{rot} \cong 2.5$ kHz [71].

423 K showed that a large amount of methylcyclohexane is selectively formed.

4.3. Synthesis of methyl-tert-butylether on acidic zeolite catalysts

Methyl-*tert*-butylether, methyl-*tert*-amylether, and ethyl-*tert*-butylether are utilized on a large scale as an octane number boosting additive in unleaded gasoline [64,65]. Methyl-*tert*-butylether, for example, is synthesized by conversion of methanol and isobutene on sulfonic acid resins, and zeolites H-Y [66–68], H-Beta [69], H-ZSM-5 [67,68], and H-[B]ZSM-5 [70] were found to be active catalysts for this reaction. To clarify the mechanism of the gas-phase synthesis of methyl-*tert*-butylether on acidic zeolites H-Y, H-ZSM-5, and H-Beta, a number *in situ* ^{13}C MAS NMR investigations under continuous-flow conditions were performed [11,71,72]. The equipment shown in Figs. 2, 3 and 6 was utilized for these studies.

As an example, Fig. 18 shows ^{13}C MAS NMR spectra recorded in the steady state of the gas-phase synthesis of methyl-*tert*-butylether from methanol and isobutene (both with ^{13}C isotopes in natural abundance) on calcined zeolite H-Beta ($n_{Si}/n_{Al} = 16$) at 333 K [71]. During the experiments, mixtures of methanol (me) and isobutene (ib) with molar ratios of 2:1 (Fig. 18a and b) and 1:1 (Fig. 18c) and modified residence times of isobutene of $W_{cat}/F_{ib} = 150$ gh/mol (Fig. 18a and b) and 75 gh/mol (Fig. 18c) were continuously injected into the MAS NMR rotor. The ^{13}C MAS NMR spectra consist of signals at 32 and 50 ppm due to methyl groups of isobutene oligomers (io) and adsorbed methanol molecules, respectively, and at 77–90 ppm assigned to surface butoxy species. Methyl groups of these butoxy species give rise to the signal at 29 ppm. The increase of the content of isobutene in the reactant flow by changing the molar methanol to isobutene ratio from 2:1 to 1:1 led to an increase of the signals at 29 ppm and 77–90 ppm (Fig. 18c), which agrees with their above-mentioned assignment. Upon purging the spent catalyst inside the MAS NMR rotor with dry nitrogen, all signals excluding those at 32 and 50 ppm disappeared (Fig. 18d). This finding indicates that alkoxy species responsible for the signals at 29 ppm and 77–90 ppm are active surface compounds and may contribute to the mechanism of the reaction under study.

An additional support for the catalytically active role of the alkoxy species at 77–90 ppm during the synthesis of methyl-*tert*-butylether on zeolite H-Beta was obtained by a simultaneous on-line gas chromatographic analysis of the volatile reaction products leaving the MAS NMR rotor (Fig. 19, top) and *in situ* MAS NMR spectroscopy of the compounds adsorbed on the catalyst under steady-state conditions (Fig. 19, bottom) [11]. These investigations showed that the intensity of the signals at 77–90 ppm correlates with the yields of methyl-*tert*-butylether determined by on-line gas chromatography. An increase of the reaction temperature of the exothermic synthesis reaction from 333 to 353 K led to a decrease of the yield of methyl-*tert*-butylether from 27% to 12%. Simultaneously, the intensity of the ^{13}C MAS NMR signals at 77–90 ppm went down [11].

By studying different zeolite catalysts under comparable reaction conditions, significantly weaker ^{13}C MAS NMR signals of alkoxy species at 77–90 ppm were found for the less active zeolites H-Y and H-ZSM-5 than for the more

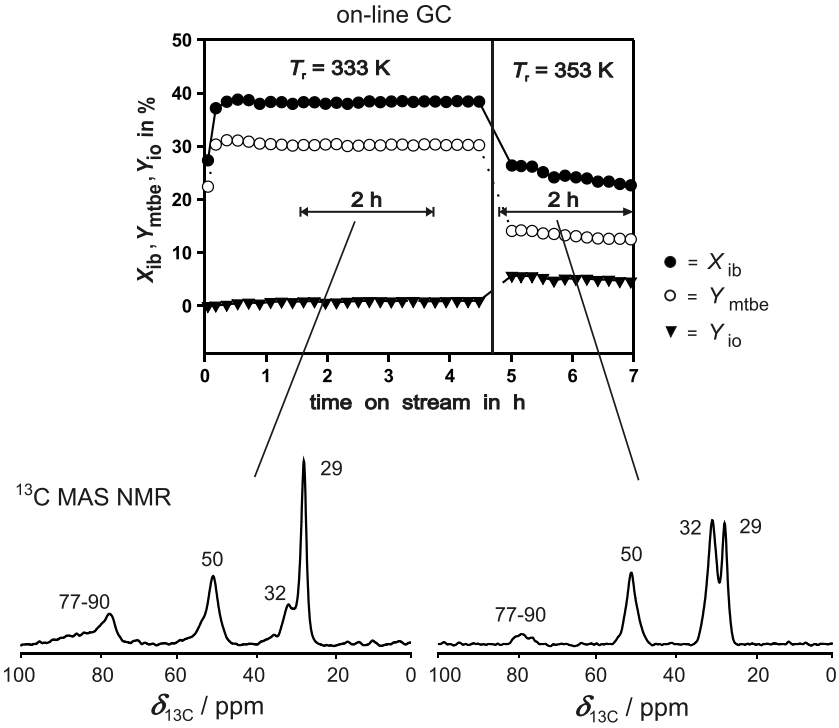


Fig. 19. ^{13}C MAS NMR spectra (bottom) of zeolite H-Beta recorded during the synthesis of methyl-*tert*-butylether (mtbe) under a continuous flow of isobutene (ib) and methanol (me) with a molar ratio of 2:1, a modified residence time of $W_{cat}/F_{ib} = 150$ gh/mol, and at reaction temperatures of 333 K (left) and 353 K (right). Simultaneously, the conversion of isobutene, X_{ib}, and yields of methyl-*tert*-butylether, Y_{mtbe}, and isobutene oligomers, Y_{io}, were determined by on-line gas chromatography (top). The NMR experiments were performed with proton high-power decoupling in a magnetic field of $B_0 = 9.4$ T, at the resonance frequency of 100.6 MHz, with the repetition time of 10 s, 720 scans per spectrum, and the sample spinning rate of $\nu_{rot} = 2.8$ kHz [11].

active zeolite H-Beta with the higher yields of methyl-*tert*-butylether [71]. This observation supports the catalytically active role of alkoxy species in the synthesis of methyl-*tert*-butylether on acidic zeolite catalysts.

4.4. Formation and decomposition of N,N,N-trimethylanilinium cations on acidic zeolite catalysts studied by stopped-flow experiments

Mono- and di-*N*-methylation of aniline are important liquid- and gas-phase reactions for the synthesis of intermediates in pharmaceutical and agricultural industry [73]. The products of the methylation of aniline by methanol are *N*-methylaniline (NMA), *N*,*N*-dimethylaniline (NNDMA), and toluidines. Mostly, the reaction mechanisms involved in the aniline methylation had been studied by analyzing the product distribution in the gas phase using gas chromatography. Therefore, *in situ* MAS NMR spectroscopy of working catalysts offers an interesting approach to reach a deeper insight into the chemical processes at the active surface sites of these materials [74–79].

Figs. 20 and 21 present investigations of the formation and decomposition of *N*,*N*,*N*-trimethylanilinium cations on zeolite catalysts performed by application of the continuous-flow and stopped-flow MAS NMR techniques [22]. The *in situ* ^{13}C MAS NMR spectra in Fig. 20 were recorded under continuous-flow conditions during methylation of aniline by methanol at reaction temperatures of 473 to 523 K. In these experiments, a mixture of aniline and ^{13}C-enriched methanol ($W_{cat}/F_{me} = 40$ gh/mol) in a molar ratio of 1:2 was injected into a modified 7 mm Doty MAS NMR probe. The weak signal at 50 ppm in Fig. 20a is due to methanol adsorbed on zeolite H-Y ($n_{Si}/n_{Al} = 2.6$), while the signals at 63.5 and 60.5 ppm indicate the formation of dimethyl ether (DME) adsorbed with side-on and end-on conformations, respectively [80,81]. After 90 min at 473 K (Fig. 20b), a new signal appeared at 39 ppm due to protonated *N*-methylaniline, i.e., *N*-methylanilinium cations ($[PhNH_2CH_3]^+$) [22]. The additional signal at 58 ppm indicates the formation of *N*,*N*,*N*-trimethylanilinium cations ($[PhN(CH_3)_3]^+$). A similar signal of quaternary ammonium cations was observed by Ernst and Pfeifer [82] at ca. 56 ppm.

Upon a further increase of the reaction temperature to 498 and 523 K, the intensity of the signal at 58 ppm due to *N*,*N*,*N*-trimethylanilinium cations increased, while the intensities of the methanol signal at 50 ppm and of the DME signals at 60.5 and 63.5 ppm decreased and eventually disappeared (Fig. 20c and d) [22]. Additional signals at 48, 21, and 16 ppm can be explained by *N*,*N*-dimethylanilinium cations ($[PhNH(CH_3)_2]^+$) and ring-alkylated ani-

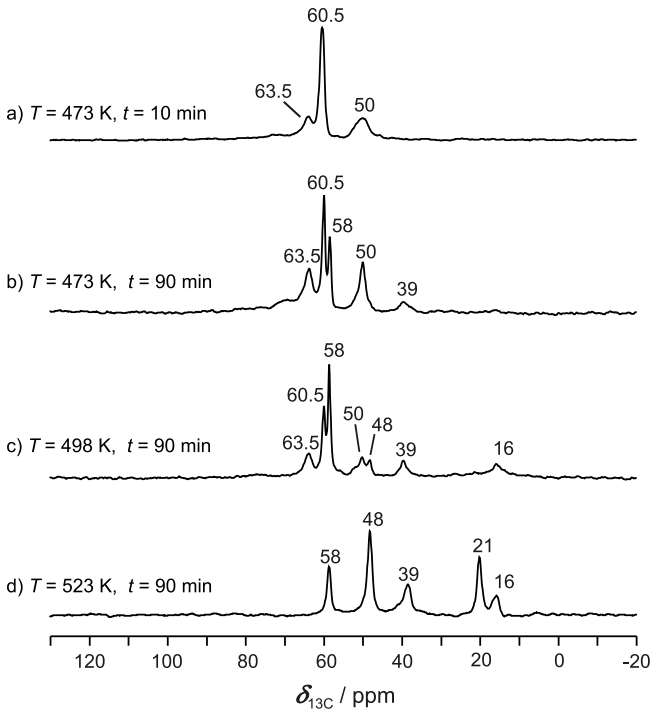


Fig. 20. ^{13}C MAS NMR spectra of zeolite H-Y recorded during methylation of aniline with methanol under continuous-flow conditions (W_{cat}/F_{me} = 40 gh/mol, methanol/aniline = 2:1) at reaction temperatures of (a, b) 473 K, (c) 473 K, and (d) 523 K. The experiments were performed with high-power proton decoupling in a magnetic field of B_0 = 9.4 T, at the resonance frequency of 100.6 MHz, with the repetition time of 5 s, 200–500 scans per spectrum, and the sample spinning rate of $\nu_{ro} \cong$ 2.0 kHz [22].

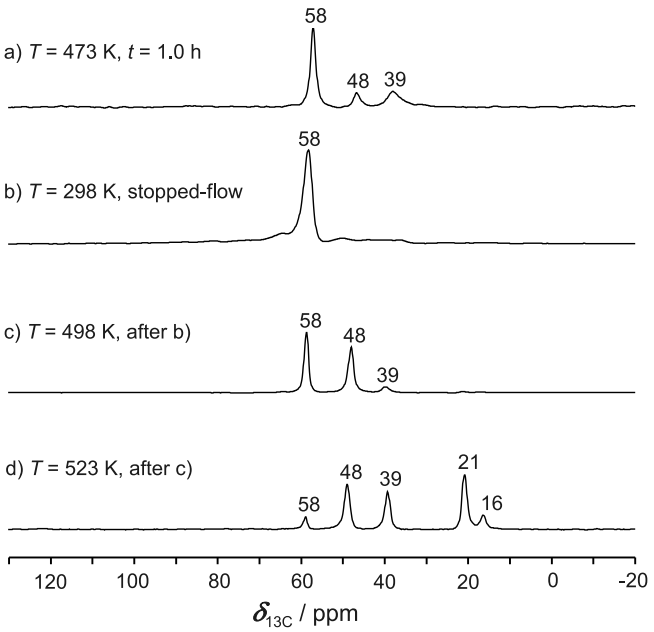


Fig. 21. ^{13}C MAS NMR spectra of zeolite H-Y recorded during methylation of aniline with methanol under continuous-flow conditions (W_{cat}/F_{me} = 75 gh/mol, methanol/aniline = 4:1) at the reaction temperatures of (a) 473 K, (b) at 298 K after stopping the flow of reactants and purging the coked catalyst with dry nitrogen, and upon heating at (c) 498 K and (d) 523 K. The experiments were performed with high-power proton decoupling in a magnetic field of B_0 = 9.4 T, at the resonance frequency of 100.6 MHz, with the repetition time of 5 s, 200–500 scans per spectrum, and the sample spinning rate of $\nu_{rot} \cong$ 2.0 kHz [22].

lines, i.e., *ortho*- and *para*-toluidine, either in their neutral or in their protonated states, respectively. Most of the above-mentioned adsorbates observed by flow ^{13}C MAS NMR spectroscopy, except the *N*,*N*,*N*-trimethylanilinium cations (58 ppm), exist in their adsorption/desorption equilibrium with the desorbed state in the gas phase.

In the second step, the role of the *N*,*N*,*N*-trimethylanilinium cations in the overall reaction was investigated by stopped-flow ^{13}C MAS NMR experiments. Once the *N*,*N*,*N*-trimethylanilinium cations were formed on zeolite H-Y under continuous-flow conditions, the reactant flow was stopped and the progressive reaction of these cations on the catalyst was investigated by *in situ* MAS NMR spectroscopy at different reaction temperatures [22].

The ^{13}C MAS NMR spectrum depicted in Fig. 21a was obtained after the continuous injection of reactants at 473 K for 1 h with a molar aniline to methanol ratio of 1:4 and a modified residence time of ^{13}C-enriched methanol of W_{cat}/F_{me} = 75 gh/mol [22]. Subsequently, the reactant flow was stopped and the zeolite catalyst was purged with dry nitrogen at ambient temperature for 1 h. The spectrum recorded at ambient temperature thereafter indicates that pure *N*,*N*,*N*-trimethylanilinium cations (58 ppm) were formed and isolated on the catalyst surface (Fig. 21b). After increasing the temperature to 498 K without starting the reactant flow again, signals occurred at 48 and 39 ppm accompanied by a decrease of the signal at 58 ppm (Fig. 21c). This observation indicates that *N*,*N*,*N*-trimethylanilinium cations were decomposed to *N*,*N*-dimethylanilinium (48 ppm) and *N*-methylanilinium cations (39 ppm). At 523 K, additional signals caused by ring-alkylated anilines appeared at 16 and 21 ppm (Fig. 21d).

Based on the results of continuous-flow and stopped-flow ^{13}C MAS NMR investigations, a mechanism for the alkylation of aniline by methanol on acidic zeolite H-Y could be proposed (Fig. 22). In the first step, methanol converts to surface methoxy groups and dimethyl ether (DME), which are the alkylating agents along with methanol. The methylation of aniline starts at 473 K and leads to a consecutive and reversible formation of *N*-methylanilinium (39 ppm), *N*,*N*-dimethylanilinium (48 ppm), and *N*,*N*,*N*-trimethylanilinium cations (58 ppm). The gas-phase products of the *N*-alkylation of aniline, i.e., *N*-methylaniline (NMA) and *N*,*N*-dimethylaniline (NNDMA), are further formed via the deprotonation of the corresponding *N*-methylanilinium and *N*,*N*-dimethylanilinium cations. The product distribution in the gas phase is, therefore, determined by the chemical equilibria between the different methylanilinium cations and by the adsorption/desorption equilibria. Furthermore, C-alkylated products (toluidines) are formed via the transformation of methylanilinium cations at reaction temperatures higher than 523 K.

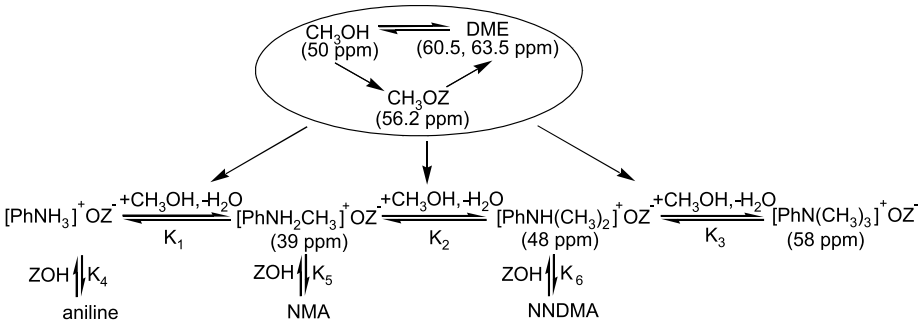


Fig. 22. Mechanism of the alkylation on aniline by methanol on acidic zeolite catalysts. K_1–K_3 are the equilibrium constants of the different methylation steps, while K_4–K_6 describe the equilibrium of the protonation and deprotonation of the reactants and reaction products in the adsorption and desorption processes [22]. Z stands for the zeolite framework.

5. Application of *in situ* flow MAS NMR-UV/Vis spectroscopy for the study of reaction mechanisms and organic deposits on solid catalysts

5.1. H/D exchange at the side-chain of ethylbenzene on acidic zeolite catalysts investigated by pulsed-flow experiments

In a number of heterogeneously catalyzed reactions (cracking, isomerization, dehydrogenation, alkylation etc.) of alkanes, the first reaction step is the activation of C–H bonds [83,84]. Investigations of the H/D exchange between reactants and Brønsted acid sites of solid catalysts at early stages of acid catalyzed reaction is a suitable approach for gaining information concerning activation mechanisms and intermediates. The main routes of these activation processes include pentavalent carbonium ions formed via direct protonation of alkanes and trivalent carbenium ions due to hydride abstraction [83–87].

Streitwieser and Reif have discussed the regioselective hydride transfer of hydrogen at the α-carbon atom (methylene group) in the side-chain of ethylbenzene under acidic conditions [88]. Recently, a preferred H/D exchange at the *β*-carbon atoms (methyl group) in the side-chain of ethylbenzene adsorbed on dealuminated zeolite H-Y was found [89]. Based on the results of *in situ* ^{1}H MAS NMR-UV/Vis spectroscopy combined with the injection of short pulses (pulsed-flow technique) of ethyl-d_5-benzene (deuterated ethyl group) onto the catalyst at reaction temperature, a reaction mechanism was suggested involving both Lewis and Brønsted acid sites in the H/D exchange reaction [89]. As an important advantage, *in situ* ^{1}H MAS NMR-UV/Vis spectroscopy can simultaneously probe routes of hydrogen transfer via characteristic ^{1}H MAS NMR signals of reactants before and after the H/D exchange and the formation of cyclohexadienyl and arylcarbenium ions via their UV/Vis bands. The application of the pulsed-flow technique (PF) allows, in the present case, the study of H/D exchange kinetics at elevated temperatures with a well-defined starting point.

The dealuminated zeolite H-Y ($n_{Si}/n_{Al} = 5.4$) used for the H/D exchange experiments was obtained by steaming zeolite H-Y ($n_{Si}/n_{Al} = 2.7$), which led to a material with 22 extra-framework aluminum species and 10.9 Brønsted acid sites per unit cell [89]. Generally, the above-mentioned extra-framework aluminum species in dealuminated zeolites Y are responsible for the Lewis acidity of these materials. Prior to the *in situ* pulsed-flow ^{1}H MAS NMR-UV/Vis experiments, the MAS NMR rotor was filled with about 100 mg of dehydrated (723 K) zeolite H-Y under dry nitrogen in a glove box and pressed to a cylindrical catalyst bed. After transferring the rotor into the MAS NMR probe, the sample was additionally dehydrated at 573 K for 1 h under dry nitrogen and then kept at the chosen reaction temperature. Subsequently, a pulse of ca. 8 mg ethyl-d_5-benzene corresponding to ca. 0.5 molecules per bridging OH group (SiOHAl) was injected into a 7 mm MAS NMR rotor using a micro pump ProMinent mikro g/5a by ProMinent Dosiertechnik, Heidelberg, Germany. With this pump, pulses of liquids with volumes of 2–50 μl can be injected.

^{1}H MAS NMR and UV/Vis spectra of dehydrated zeolite H-Y recorded 10–15 min after the injection of ethyl-d_5-benzene are shown in Fig. 23 [89]. The ^{1}H MAS NMR signals at 1.2, 2.7, and 7.3 ppm (Fig. 23a) arise from hydrogen atoms in side-chain methyl and methylene groups and in the non-deuterated aromatic rings, respectively, of ethyl-d_5-benzene. The signals of non-deuterated bridging OH groups (SiOHAl) acting as Brønsted acid site of the zeolite catalyst are too weak and broad to be observed under the conditions applied. Upon adsorption of ethyl-d_5-benzene on zeolite H-Y at temperatures of 393–423 K, the ^{1}H MAS NMR spectra consist exclusively of signals of hydrogen atoms in the non-deuterated aromatic ring (7.3 ppm). Simultaneously recorded UV/Vis spectra (right) show bands at 270 and 400 nm due to neutral aromatics (ethylbenzene) and ethylcyclohexadienyl carbenium ions, respectively (Fig. 23b) [90]. The latter species are caused by a ring protonation of the ethylbenzene molecules (strong UV/Vis band at 400 nm), which is an intermediate step of the exchange of hydrogen atoms bound to ring carbon atoms

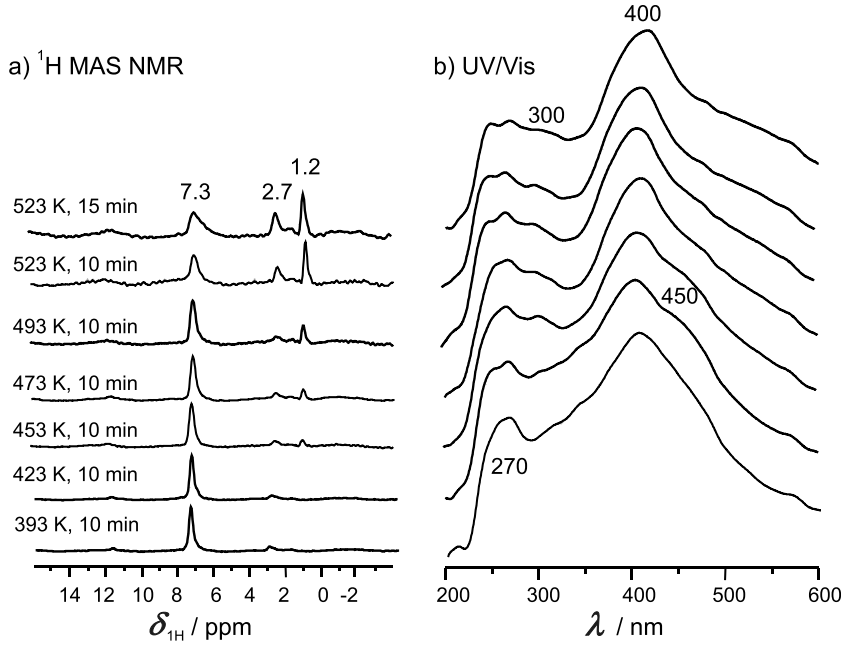


Fig. 23. ^{1}H MAS NMR (a) and UV/Vis spectra (b) recorded during the H/D exchange of ethyl-d_5-benzene ($C_6H_5C_2D_5$) on dealuminated zeolite H-Y ($n_{Si}/n_{Al} = 5.4$) upon a pulse-wise adsorption of the reactant molecules. The experiments were performed in a magnetic field of $B_0 = 9.4$ T, at the resonance frequency of 400.1 MHz, with the repetition time of 10 s, 32 scans per spectrum, and the sample spinning rate of $\nu_{rot} \cong 2.0$ kHz [89].

with the hydroxyl protons of SiOHAl groups occurring in the temperature range of 393–423 K [91].

At 453 K, the ^{1}H MAS NMR signal of methyl groups appears at 1.2 ppm (Fig. 23a) and increases in intensity at higher temperatures. Hence, there is a preferred H/D exchange of Brønsted acid sites in dealuminated zeolite H-Y with the methyl groups of the side-chains of ethyl-d_5-benzene molecules. Simultaneously, a broad UV/Vis band occurs at ca. 450 nm (Fig. 23b) indicating the formation of sec-ethylphenyl carbenium ions ($C_6H_5(CD)^+CD_3$) [90,92]. Finally, raising the temperature to 493 K and higher is accompanied by a further increase of the ^{1}H MAS NMR signal at 1.2 ppm and by the appearance of the signal of methylene groups at 2.7 ppm. The dealkylation/realkylation reactions of the ethyl group at aromatic compounds are responsible for the experimentally observed simultaneous increase of the signals at 1.2 and 2.7 ppm.

To study the activation energy of the regioselective H/D exchange on zeolite H-Y at 443–463 K, *in situ* pulsed-flow ^{1}H MAS NMR experiments were performed. As an example, Fig. 24a shows ^{1}H MAS NMR spectra recorded upon injection of ethyl-d_5-benzene onto zeolite H-Y at 453 K. The Arrhenius plot of the H/D exchange rates of methyl groups at 1.2 ppm is given in Fig. 24b. The activation energy of the regioselective H/D exchange of the methyl group of the side-chain of ethyl-d_5-benzene was determined to be 194 ± 23 kJ/mol. This value is in good agreement with the calculated value of 202.6 kJ/mol for hydride transfer reactions between alkanes and carbenium ions [93].

A mechanism involving both Brønsted and Lewis acid sites was suggested [89] to explain the ^{1}H MAS NMR signals and UV/Vis bands experimentally observed during the

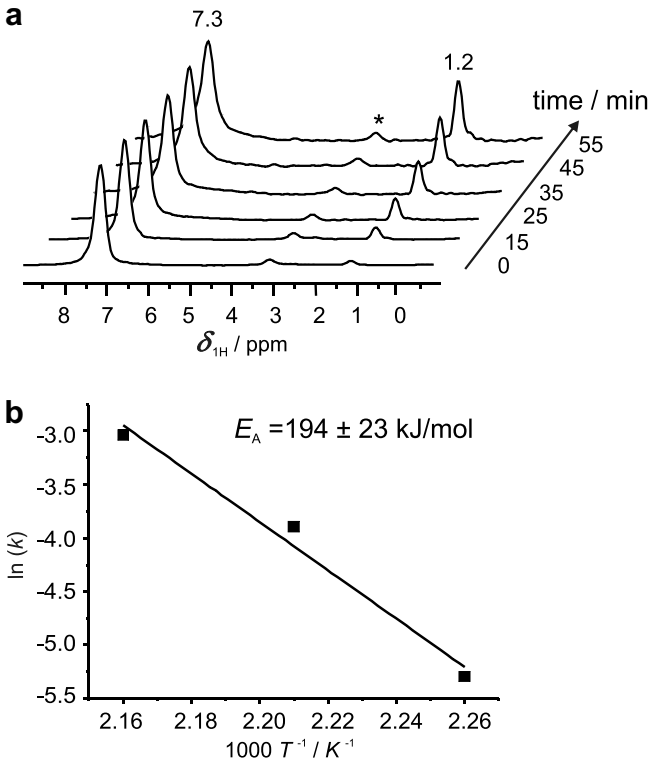


Fig. 24. (a) Stack plot of ^{1}H MAS NMR spectra recorded during the H/D exchange of ethyl-d_5-benzene ($C_6H_5C_2D_5$) on dehydrated (723 K) zeolite H-Y at 453 K. (b) Arrhenius plot of the H/D exchange rates of the methyl group of ethyl-d_5-benzene ($C_6H_5C_2D_5$) adsorbed on zeolite H-Y at temperatures of 443, 453, and 463 K [89]. The spectra were recorded as described in the caption of Fig. 23.

regioselective H/D exchange of ethyl-d_5-benzene on dealuminated zeolite H-Y at 443–463 K and the activation energy of 194 kJ/mol obtained for the H/D exchange kinetics of the side-chain methyl group. At first, a hydride abstraction on Lewis acid sites leading to the sec-ethylphenyl carbenium ion $C_6H_5(CD)^+CD_3$ occurs. The formation of this surface species is indicated by the UV/Vis band 450 nm. The next step is a deprotonation leading to the formation of styrene (UV/Vis band at 300 nm) as an intermediate, which is followed by a protonation causing the sec-ethylphenyl carbenium ion $C_6H_5(CD)^+CHD_2$. According to Markovnikov's rule, the protonation occurs preferentially at the β-carbon responsible for the regioselective H/D exchange of the methyl group. Subsequent intermolecular hydride (D^-) transfer from another reactant molecule to the sec-ethylphenyl carbenium ion $C_6H_5(CD)^+CHD_2$ leads to the ethylbenzene with H/D-exchanged methyl group responsible for the ^1H MAS NMR signal at 1.2 ppm. The intermolecular hydride transfer is the rate determining step and causes the experimentally obtained activation energy of 194 kJ/mol [89].

5.2. Organic deposits formed on H-SAPO-34 during the methanol-to-olefin conversion

The industrial demand for light olefins, such as ethene and propene, causes an increasing interest in the conversion of methanol-to-olefins (MTO) on acidic zeolite catalysts [55]. A number of studies performed during the past decades focused on the mechanism of the methanol-to-olefin reaction. As indicated by previous studies of the MTO process (see, e.g., Refs. [55,94–97]), the conversion of an equilibrium mixture of methanol and dimethyl ether is dominated by a hydrocarbon-pool route in which methanol is added to reactive organic compounds formed in the pores of acidic zeolite catalysts. Depending on the catalyst and reaction conditions used, these compounds can be branched olefins, polyalkylbenzenzes, cyclic carbenium ions, and polyalkylbenzenium cations. The elimination of alkyl groups from these hydrocarbon-pool compounds produces the light olefins [55,94–97].

There is still considerable debate on the details of the mechanism of the MTO reaction and on the reasons for catalyst deactivation. Therefore, a significant effort is made to elucidate the phenomenon of hydrocarbon formation on zeolite catalysts by *in situ* FT-IR [98], MAS NMR [44,99], EPR [100], and UV/Vis spectroscopy [101], partially coupled with on-line gas chromatography or mass spectrometry. ^{13}C MAS NMR spectroscopy is able to provide a suitable separation and assignment of signals of organic deposits on zeolite catalysts and allows a quantification of spectra [44]. UV/Vis spectroscopy possesses a high sensitivity for characteristic hydrocarbon-pool compounds and coke deposits of the MTO conversion, such as molecules with conjugated double bonds, aromatics, and unsaturated carbenium ions [101]. Therefore, the MAS NMR-UV/Vis technique described in Sections 2.3 and 5.1 offers an interesting approach for studying the formation of organic deposits and coke compounds on working zeolite catalysts at the steady state of the MTO process.

Upon transferring the rotor filled with the calcined catalyst into the flow MAS NMR-UV/Vis probe and a secondary dehydration of this material, a continuous flow of ^{13}C-enriched methanol with a modified residence time of $W_{cat}/F_{me} = 25$ gh/mol was injected into the 7 mm flow MAS NMR probe. The studies of the MTO process shown in Fig. 25 were performed with H-SAPO-34 (CHA-type structure, CHA: chabazite [52]) as acidic catalyst. The continuous-flow ^{13}C MAS NMR and UV/Vis spectra were recorded during the conversion of methanol on H-SAPO-34 at reaction temperatures of 473 (a) to 673 K (d). Simultaneously, the yields of volatile reaction products, such as dimethyl ether (DME), ethene ($C_{2=}$), propene ($C_{3=}$), and butenes ($C_{4=}$), were analyzed by on-line gas chromatography (given on the left-hand side of Fig. 25).

At the reaction temperatures of 473 K and 523 K (Fig. 25a and b), the conversion of methanol on H-SAPO-34 is dominated by the formation of DME, which is indicated by on-line gas chromatographic data and by ^{13}C MAS NMR signals of adsorbed methanol (50 ppm) and DME (61 ppm). Simultaneously obtained UV/Vis spectra of organic deposits formed on the zeolite catalyst are depicted on the right-hand side of Fig. 25. UV/Vis sensitive species are formed first at 413 K and cause a weak band at 245 nm, which is assigned to dienes [102,103].

Upon increasing the reaction temperature to 573 K (Fig. 25c), most of the methanol and DME molecules are converted to other products. New ^{13}C MAS NMR signals appear in the region of alkyl groups at 10–40 ppm and of aromatic compounds at 125–135 ppm [104], which indicate the formation of polyalkylaromatics. On-line gas chromatographic analysis of the volatile reaction products shows a strong increase in the yields of light olefins. The UV/Vis spectrum obtained at 573 K consists of a dominating band at ca. 300 nm due to monoenylic carbenium ions [102,103]. Furthermore, additional bands appear as weak shoulders at ca. 280 and 345 nm, which can be assigned to polyalkylaromatics and dienylic carbenium ions [105].

At the reaction temperature of 623 K (Fig. 25d), the high-field range of the ^{13}C MAS NMR spectrum is dominated by a signal at 18 ppm due to methyl groups bound to aromatics, while most of the other signals in the region of alkyl groups observed at lower reaction temperatures disappeared. Simultaneously, the ^{13}C MAS NMR signals of aromatic compounds at 125–135 ppm increased. The UV/Vis spectrum obtained at this temperature is dominated by a band at 280 nm with shoulders at 300 and 345 nm due to polyalkylaromatics and monoenylic and dienylic carbenium ions, respectively. In addition, a broad band appeared at 430 nm, which is generally explained by trienylic carbenium ions. These carbenium ions could be precursors of coke compounds responsible for the catalyst deactivation [105], and in agreement with this, the UV/Vis spectrum recorded at 673 K (Fig. 25e) shows a strong band

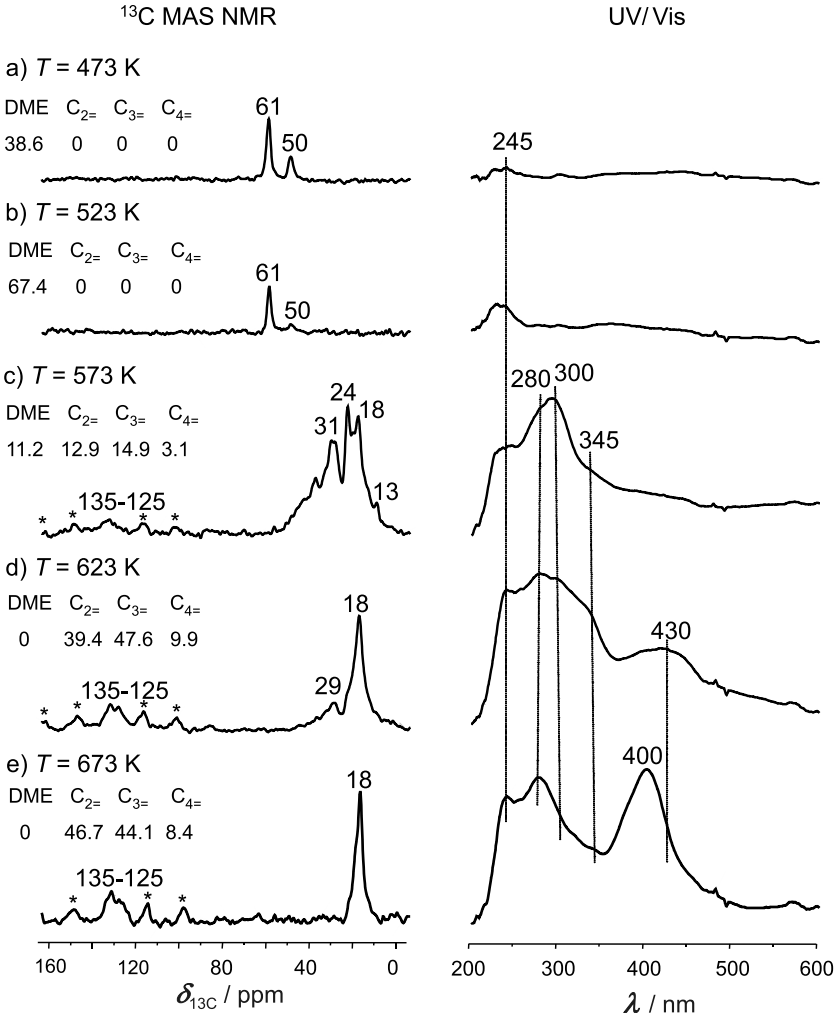


Fig. 25. ^{13}C MAS NMR (left) and UV/Vis spectra (right) recorded during the conversion of ^{13}C-enriched methanol ($W_{cat}/F_{me} = 25$ gh/mol) on H-SAPO-34 at reaction temperatures of (a) 47 K to (d) 673 K. On the left-hand side, the yields of dimethyl ether (DME), ethene ($C_{2=}$), propene ($C_{3=}$), and butenes ($C_{4=}$) as determined by on-line gas chromatography are given in %. Asterisks denote spinning sidebands. The NMR experiments were performed with high-power proton decoupling in a magnetic field of $B_0 = 9.4$ T, at the resonance frequency of 100.6 MHz, with the repetition time of 5 s, 200–500 scans per spectrum, and the sample spinning rate of $\nu_{rot} \cong 2.0$ kHz [28].

at 400 nm due to polycyclic aromatics acting as coke compounds. The simultaneously recorded ^{13}C MAS NMR spectrum consists of signals at 18 and ca. 135 ppm due to polymethylaromatics [104]. In agreement with the occurrence of the UV/Vis band at 400 nm, the broad ^{13}C MAS NMR signal at ca. 125 ppm also indicates the formation of polycyclic aromatics.

5.3. Quantitative investigations of the regeneration of coked MTO catalysts

An important advantage of solid-state NMR spectroscopy is the possibility of a direct quantitative evaluation of signal intensities in order to determine the concentrations of the species under study. In the case of *in situ* solid-state NMR spectroscopy of adsorbate complexes and deposits formed on solid catalysts, the most accurate procedure is a stopped-flow experiment and a subsequent measurement of the signal intensities at room temperature. In the case of measurements at elevated temperatures, Curie's law and the effect of heating of the radio frequency coil on the signal intensity have to be considered.

As an example of stopped-flow experiments for performing quantitative solid-state NMR studies, Fig. 26a presents the ^{13}C MAS NMR spectrum of H-SAPO-34 obtained at room temperature upon methanol-to-olefin conversion at 673 K for 3 h [28]. As indicated by the band at 400 nm in the simultaneously recorded UV/Vis spectrum (Fig. 26, right), the corresponding catalyst is strongly coked, i.e., covered by polycyclic aromatics. The concentration of ^{13}C atoms in organic deposits and the number of aromatic compounds per chabazite cage ($T_{12}O_{24}$, weight of 1.38 mmol/g) were determined by the simulation of the spectral range of ^{13}C MAS NMR signals of alkyl groups and aromatic rings. The corresponding ^{13}C MAS NMR intensities were compared with the intensity of an external intensity standard prepared by adsorption of a certain amount of ^{13}C-enriched methanol on dehydrated H-SAPO-34 [28].

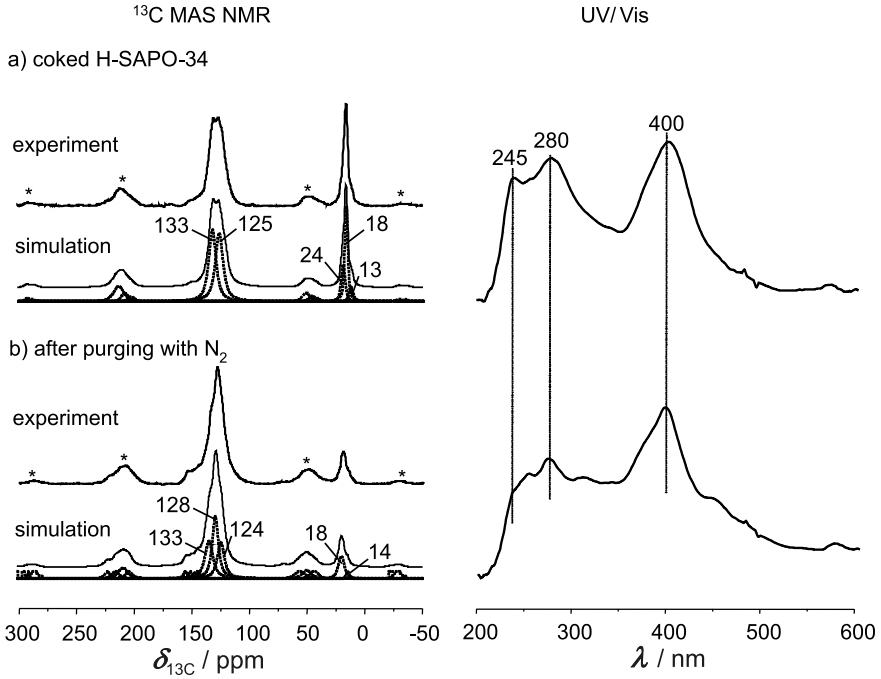


Fig. 26. ^{13}C MAS NMR (left) and UV/Vis spectra (right) of H-SAPO-34 recorded at room temperature (a) after methanol conversion at 673 K, (b) after subsequent purging with nitrogen (30 ml/min) at 673 K. Asterisks denote spinning sidebands. The NMR experiments were performed with high-power proton decoupling in a magnetic field of $B_0 = 9.4$ T, at the resonance frequency of 100.6 MHz, with the repetition time of 30 s, 200 scans per spectrum, and the sample spinning rate of $\nu_{rot} \cong 8.0$ kHz [28].

Table 2 gives a survey of the chemical shift ranges (column 1) and assignments of ^{13}C MAS NMR signals (column 2) in the spectra of the H-SAPO-34 catalyst coked by methanol conversion at 673 K. In column 3 of Table 2, the concentration of ^{13}C atoms in alkyl groups and aromatic rings of the organic deposits formed by conversion of methanol are given. The number of methyl groups bound to aromatics is significantly higher than those of ethyl groups. This finding shows that polymethylbenzene molecules are the dominating hydrocarbon-pool compounds of the MTO process on H-SAPO-34. Upon methanol conversion at 673 K, aromatic compounds with 3.33 mmol of ^{13}C atoms or 0.61 mmol of aromatic rings per gram of catalyst were formed corresponding to ca. 1.1 aromatic rings per chabazite cage. These aromatic compounds are alkylated by 0.69 mmol of methyl and ethyl groups per gram of catalyst corresponding to ca. 1.1 alkyl groups per aromatic ring. The composition of the organic deposits are characterized by a low number of alkyl groups corresponding to typical coke compounds, which is supported by the strong UV/Vis band at 400 nm due to polycyclic aromatics (Fig. 26a, right).

In order to study the thermal stability of the organic deposits on H-SAPO-34, the catalyst was purged with dry nitrogen at 673 K for 2 h. Fig. 26b, left, shows the ^{13}C MAS NMR spectrum of this purged catalyst. The results of the quantitative evaluation are summarized in column 4 of Table 2. As indicated by these values, the number of ^{13}C atoms in aromatic compounds decreased slightly to 2.45 mmol g^{-1} corresponding to ca. 0.3 aromatic rings per chabazite cage. Also the number of alkyl groups decreased to 0.34 mmol g^{-1} corresponding to 0.8 alkyl

Table 2
Quantitative evaluation of the ^{13}C MAS NMR signals of organic deposits on H-SAPO-34 upon conversion of ^{13}C-enriched methanol at 673 K under continuous-flow (CF) conditions with the residence time of $W_{cat}/F_{me} = 25$ gh/mol, subsequent purging by dry nitrogen (30 ml/min) at 673 K for 2 h, and regeneration by synthetic air (syn. air, 20 vol.% oxygen, 30 ml/min) at 673 and 773 K for 2 h [28]

Signal at δ_{13C}/ppm	Assignments	Concentration of ^{13}C atoms (mmol g^{-1})			
		Methanol CF at 673 K	N_2 at 673 K	Syn. air at 673 K	Syn. air at 773 K
16–21	Methyl groups bound to aromatics	0.53	0.31	–	–
14–15 and 22–29	Ethyl groups bound to aromatics	0.16	0.06	–	–
125–135	Alkylated and non-alkylated aromatics	3.33	2.45	1.04	0.31
145–155	At ring positions of aromatics bound to hydroxyl groups	–	–	0.45	0.13

The assignments of ^{13}C MAS NMR signals were performed according to Ref. [104]. The accuracy of the spin concentration is ±10%.

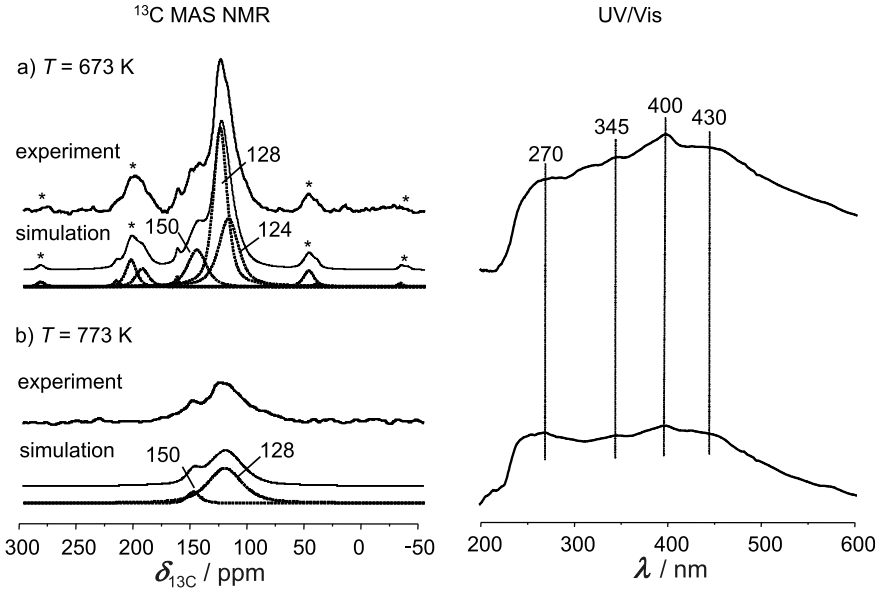


Fig. 27. ^{13}C MAS NMR (left) and UV/Vis spectra (right) of H-SAPO-34 recorded at room temperature after methanol conversion at 673 K and subsequent purging with synthetic air (20 vol.% oxygen, 30 ml/min) at (a) 673 K and (b) 773 K. Asterisks denote spinning sidebands. The NMR experiments were performed with high-power proton decoupling in a magnetic field of $B_0 = 9.4$ T, at the resonance frequency of 100.6 MHz, with the repetition time of 30 s, 200 scans per spectrum, and the sample spinning rate of $\nu_{rot} \cong 8.0$ kHz [28].

groups per aromatic ring. This corresponds to a decrease of the organic deposits by 25–27% in comparison with the coked catalyst before purging with dry nitrogen at 673 K. In the simultaneously recorded UV/Vis spectra, the main change is a decrease of the bands of polyalkyl aromatics at 280 nm and the shoulder at 245 nm due to dienes (compare Fig. 26a and b, right). This behavior corresponds to a smaller number of polyalkylaromatics as observed by ^{13}C MAS NMR spectroscopy. On the other hand, the large band at 400 nm indicates that polycyclic aromatics on the coked H-SAPO-34 catalyst exhibit a high thermal stability and are not affected by purging with nitrogen.

Often, catalysts deactivated by coke are regenerated by burning off the organic deposits in the presence of oxygen [55,106]. Therefore, the coked H-SAPO-34 catalyst obtained upon methanol conversion at 673 K was treated with synthetic air (20 vol.% oxygen) at 673 and 773 K for 2 h. Again, the effect of this treatment on the organic deposits was investigated by ^{13}C MAS NMR-UV/Vis spectroscopy. Fig. 27, left, shows the ^{13}C MAS NMR spectra of the coked H-SAPO-34 catalyst recorded upon purging with synthetic air for 2 h. After the treatment at 673 K, a significant removal of all polyalkylaromatics occurred (Fig. 27a, left, and column 5 of Table 2). In comparison with the coked H-SAPO-34 catalyst, which was not treated with synthetic air (column 3 of Table 2), the number of ^{13}C atoms in aromatic rings of the organic deposits was decreased by ca. 69%. This is accompanied by a strong decrease of the UV/Vis band of polycyclic aromatics at 400 nm (Fig. 27a, right). The UV/Vis band of polyalkylaromatics at 280 nm disappeared totally, which agrees with the results of ^{13}C MAS NMR spectroscopy. In addition, new ^{13}C MAS NMR signals occurred at 145–155 ppm. These signals indicate a partial hydroxylation of remaining aromatic compounds during the treatment with synthetic air. In the UV/Vis spectra, these phenolic species are responsible for the new band at ca. 270 nm [103]. After raising the regeneration temperature to 773 K there is a decrease in the number of ^{13}C atoms in aromatic rings of organic deposits by 90% in comparison with the non-purged H-SAPO-34 catalyst (Fig. 27b, left and column 7 of Table 2). Likewise, the UV/Vis band of neutral polycyclic aromatics at 400 nm became weaker (Fig. 27b, right).

In summary, stopped-flow MAS NMR experiments combined with the evaluation of signal intensities at room temperature is a suitable procedure for a quantification of the concentration of the products formed under steady-state conditions in a heterogeneously catalyzed reaction. Data obtained in this way allow the investigation of the changes of deposits on solid catalysts upon specific treatments, such as catalyst regeneration. Simultaneously recorded UV/Vis spectra support the assignment of signals observed by solid-state NMR spectroscopy.

6. Conclusions

This review demonstrates that *in situ* MAS NMR spectroscopy under flow conditions is able to provide important and novel information on the nature and properties of surface sites on solid catalysts and the mechanisms of heterogeneously catalyzed reactions. In the past decade, a number of new techniques have been introduced and applied to experiments under continuous-flow, switched-flow, stopped-flow, and pulsed-flow conditions. Depending on the scientific problem being investigated, these experimental techniques provide useful approaches for the study

of working catalysts and of surface compounds formed on these materials under reaction conditions.

The limited signal-to-noise ratio of NMR signals is a significant problem, especially at elevated temperatures. The central aim of research in this field should be, therefore, the enhancement of the sensitivity of *in situ* MAS NMR spectroscopy, e.g., by an enhancement of the nuclear polarization of reactants and surface compounds by utilizing hyperpolarized xenon. Last but not least, interesting new information on the nature of working catalysts and the mechanisms of heterogeneously catalyzed reactions can be expected, if *in situ* flow MAS NMR spectroscopy is combined with other analytical techniques, such as has already been demonstrated with gas chromatography, mass spectrometry, and UV/Vis spectroscopy.

Acknowledgements

Financial support by Deutsche Forschungsgemeinschaft, Fonds der Chemischen Industrie, and Volkswagenstiftung is gratefully acknowledged.

References

[1] (a) G.W. Haddix, J.A. Reimer, A.T. Bell, J. Catal. 106 (1987) 111; (b) G.W. Haddix, J.A. Reimer, A.T. Bell, J. Catal. 108 (1987) 50.
[2] M.E. Davis, P. Hathaway, D. Morgan, T. Glass, H. Dorn, Stud. Surf. Sci. Catal. 38 (1988) 263.
[3] A.M. Beale, A.M.J. van der Eerden, K. Kervinen, M.A. Newton, B.M. Weckhuysen, Chem. Commun. (2005) 3015.
[4] B.M. Weckhuysen, Chem. Commun. (2002) 97.
[5] M. Hunger, J. Weitkamp, in: B.M. Weckhuysen (Ed.), In-situ Spectroscopy of Catalysts, American Scientific Publishers, Stevenson Ranch, CA, 2004, p. 177.
[6] M. Hunger, Microporous Mesoporous Mater. 82 (2005) 241.
[7] W. Wang, Y. Jiang, M. Hunger, Catal. Today 113 (2006) 102.
[8] M. Hunger, W. Wang, Adv. Catal. 50 (2006) 149.
[9] M. Hunger, T. Horvath, J. Chem. Soc., Chem. Commun. (1995) 1423.
[10] M. Hunger, T. Horvath, J. Catal. 167 (1997) 187.
[11] M. Hunger, M. Seiler, T. Horvath, Catal. Lett. 57 (1999) 199.
[12] A. Buchholz, W. Wang, A. Arnold, M. Xu, M. Hunger, Microporous Mesoporous Mater. 57 (2003) 157.
[13] A. Buchholz, W. Wang, M. Xu, A. Arnold, M. Hunger, J. Phys. Chem. B 108 (2004) 3107.
[14] H. Mori, H. Kono, M. Terano, A. Nossov, V.A. Zakharov, Macromol. Rapid Commun. 20 (1999) 536.
[15] A. Nossov, F. Guenneau, M.-A. Springuel-Huet, E. Haddad, V. Montouillout, B. Knott, F. Engelke, C. Fernandez, A. Gedeon, Phys. Chem. Chem. Phys. 5 (2003) 4479.
[16] V. Sundaramurthy, J.-P. Cognec, K. Thomas, B. Knott, F. Engelke, C. Fernandez, C.R. Chimie 9 (2006) 459.
[17] P. Goguen, J.F. Haw, J. Catal. 161 (1996) 870.
[18] P.K. Isbester, A. Zalusky, D.H. Lewis, M.C. Douskey, M.J. Pomije, K.P. Mann, E.J. Munson, Catal. Today 49 (1999) 363.
[19] P.K. Isbester, L. Kaune, E.J. Munson, Chem. Tech. (November) (1999) 40.
[20] C. Keeler, J. Xiong, H. Lock, S. Dec, T. Tao, G.E. Maciel, Catal. Today 49 (1999) 377.
[21] N.M. Szeverenyi, A. Bax, G.E. Maciel, J. Magn. Reson. 61 (1985) 440.
[22] W. Wang, M. Seiler, I.I. Ivanova, U. Sternberg, J. Weitkamp, M. Hunger, J. Am. Chem. Soc. 124 (2002) 7548.
[23] M. Seiler, W. Wang, A. Buchholz, M. Hunger, Catal. Lett. 88 (2003) 187.
[24] W. Wang, M. Xu, A. Buchholz, A. Arnold, M. Hunger, Magn. Reson. Imaging 21 (2003) 329.
[25] M. Maiwald, H.H. Fischer, Y.-K. Kim, K. Albert, J. Magn. Reson. 166 (2004) 135.
[26] M. Hunger, W. Wang, Chem. Commun. (2004) 584.
[27] Y. Jiang, W. Wang, V.R. Reddy Marthala, J. Huang, B. Sulikowski, M. Hunger, J. Catal. 238 (2006) 21.
[28] Y. Jiang, J. Huang, V.R. Reddy Marthala, Y.S. Ooi, J. Weitkamp, M. Hunger, Microporous Mesoporous Mater. 105 (2007) 132.
[29] I.L. Moudrakovski, A. Nossov, S. Lang, S.R. Breeze, C.I. Ratcliffe, B. Simard, G. Santyr, J.A. Ripmeester, Chem. Mater. 12 (2000) 1181.
[30] D. Raftery, E. MacNamara, G. Fisher, C.V. Rice, J. Smith, J. Am. Chem. Soc. 119 (1997) 8746.
[31] (a) M. Haake, A. Pines, J.A. Reimer, R. Seydoux, J. Am. Chem. Soc. 119 (1997) 11711; (b) E. Brunner, R. Seydoux, M. Haake, A. Pines, J.A. Reimer, J. Magn. Reson. 130 (1998) 145.
[32] E. MacNamara, G. Fisher, J. Smith, C.V. Rice, S.-J. Hwang, D. Raftery, J. Phys. Chem. B 103 (1999) 1158.
[33] R. Seydoux, A. Pines, M. Haake, J.A. Reimer, J. Phys. Chem. B 103 (1999) 4629.
[34] A. Abragam, Principles of Nuclear Magnetism, Oxford Science Publications, Clarendon Press, Oxford, 1994, pp. 110 and 140.
[35] A. Bielecki, D.P. Burum, J. Magn. Reson. A 116 (1995) 215.
[36] A.E. Aliev, K.D.M. Harris, Magn. Reson. Chem. 32 (1994) 366.
[37] G.-J.M.P. van Moorsel, E.R.H. van Eck, C.P. Grey, J. Magn. Reson. A 113 (1995) 159.
[38] T. Takahashi, H. Kawashima, H. Sugisawa, T. Baba, Solid State Nucl. Magn. Reson. 15 (1999) 119.
[39] G. Campbell, R.C. Crosby, J.F. Haw, J. Magn. Reson. 69 (1986) 191.
[40] J.F. Haw, R.A. Crook, R.C. Crosby, J. Magn. Reson. 66 (1986) 551.
[41] B. Wehrle, F. Aguilar-Parrilla, H.-H. Limbach, J. Magn. Reson. 87 (1990) 584.
[42] H.-J. Pan, B.C. Gerstein, J. Magn. Reson. 92 (1991) 618.
[43] D.B. Ferguson, J.F. Haw, Anal. Chem. 67 (1995) 3342.
[44] M. Seiler, U. Schenk, M. Hunger, Catal. Lett. 62 (1999) 139.
[45] T. Ito, J. Fraissard, J. Phys. Chem. 76 (1982) 5225.
[46] J. Ripmeester, J. Am. Chem. Soc. 104 (1982) 289.
[47] P.J. Barrie, J. Klinowski, Progr. NMR Spectrosc. 24 (1992) 91.
[48] J.L. Bonardet, J. Fraissard, A. Gedeon, M.A. Springuel-Huet, Catal. Rev. 41 (1999) 117.
[49] A. Nossov, E. Haddad, F. Guenneau, C. Mignon, A. Gedeon, D. Grosso, F. Babonneau, C. Bonhomme, C. Sanchez, Chem. Commun. (2002) 2476.
[50] I.L. Moudrakovski, S. Lang, C.I. Ratcliffe, B. Simard, G. Santyr, J.A. Ripmeester, J. Magn. Reson. 144 (2000) 372.
[51] A. Corma, U. Diaz, M.E. Domine, V. Fornes, J. Am. Chem. Soc. 122 (2000) 2804.
[52] Ch. Baerlocher, W.M. Meier, D.H. Olson, Atlas of Zeolite Framework Types, 5th revised ed., Elsevier, Amsterdam, 2001.
[53] J. Jeener, B.H. Meier, P. Bachmann, R.R. Ernst, J. Chem. Phys. 71 (1979) 4546.
[54] M. Hunger, M. Anderson, A. Ojo, H. Pfeifer, Microporous Mater. 1 (1993) 17.
[55] M. Stoecker, Microporous Mesoporous Mater. 29 (1999) 3.
[56] J.A. Martens, P.J. Grobet, P.A. Jacobs, J. Catal. 126 (1990) 299.
[57] H.B. Mostad, M. Stoecker, A. Karlsson, T. Rorvik, Appl. Catal. A: Gen. 144 (1996) 305.
[58] C. Minchev, Y. Neinska, V. Valtchev, V. Minkov, T. Tsoncheva, V. Penchev, H. Lechert, M. Hess, Catal. Lett. 18 (1993) 125.
[59] M. Briend, A. Shikholeslami, M.J. Peltre, D. Delafosse, D. Barthomeuf, J. Chem. Soc. Dalton Trans. (1989) 1361.
[60] M. Hunger, D. Freude, H. Pfeifer, J. Chem. Soc., Faraday Trans. 87 (1991) 657.

[61] P. Batamack, C. Doremieux-Morin, J. Fraissard, D. Freude, J. Phys. Chem. 95 (1991) 3790.
[62] G. Ertl, H. Knoezinger, J. Weitkamp, Handbook of Heterogeneous Catalysis, vol. 5, Wiley-VCH, Weinheim, 1997, pp. 2140 and 2165.
[63] J.C. Duchet, D. Guillaume, A. Monnier, C. Dujardin, J.P. Gilson, J. Van Gestel, G. Szabo, P. Nascimento, J. Catal. 198 (2001) 328.
[64] G. Ertl, H. Knoezinger, J. Weitkamp, Handbook of Heterogeneous Catalysis, vols. 4 and 3, Wiley-VCH, Weinheim, 1997, pp. 1484 and 1986.
[65] J.G. Goodwin, S. Natesakhawat, A.A. Nikolopoulos, S.Y. Kim, Catal. Rev. Sci. Eng. 44 (2002) 287.
[66] A. Kogelbauer, J.G. Goodwin, J.A. Lercher, J. Phys. Chem. 99 (1995) 8777.
[67] A. Kogelbauer, A.A. Nikolopoulos, J.G. Goodwin, G. Marcelin, J. Catal. 152 (1995) 122.
[68] A.A. Nikolopoulos, R. Oukaci, J.G. Goodwin, G. Marcelin, Catal. Lett. 27 (1994) 149.
[69] F. Collignon, M. Mariani, S. Moreno, M. Remy, G. Poncelet, J. Catal. 166 (1997) 53.
[70] W.F. Hoelderich, in: S. Yoshida (Ed.), Catalytic Science and Technology, vol. 1, Kodancha Ltd, 1991, p. 31.
[71] T. Horvath, M. Seiler, M. Hunger, Appl. Catal. A: Gen. 193 (2000) 227.
[72] M. Hunger, T. Horvath, J. Weitkamp, Microporous Mesoporous Mater. 22 (1998) 357.
[73] G. Ertl, H. Knoezinger, J. Weitkamp, Handbook of Heterogeneous Catalysis, vol. 5, Wiley-VCH, Weinheim, 1997.
[74] I.I. Ivanova, E.B. Pomakhina, A.I. Rebrov, M. Hunger, Yu.G. Kolyagin, J. Weitkamp, J. Catal. 203 (2001) 375.
[75] I.I. Ivanova, O.A. Ponomoreva, E.B. Pomakhina, E.E. Knyazeva, V.V. Yuschenko, M. Hunger, J. Weitkamp, Stud. Surf. Sci. Catal. 142 (2002) 659.
[76] I.I. Ivanova, O.A. Ponomoreva, A.I. Rebrov, W. Wang, M. Hunger, J. Weitkamp, Kinetics Catal. 44 (5) (2003) 701.
[77] W. Wang, M. Seiler, I.I. Ivanova, J. Weitkamp, M. Hunger, Chem. Commun. (2001) 1362.
[78] I.I. Ivanova, E.B. Pomakhina, I.B. Borodina, A.I. Rebrov, W. Wang, J. Weitkamp, M. Hunger, Stud. Surf. Sci. Catal. 154 (2004) 2221.
[79] I.I. Ivanova, N.S. Nesterenko, C. Fernandez, Catal. Today 113 (2006) 115.
[80] I.I. Ivanova, A. Corma, J. Phys. Chem. B 101 (1997) 547.
[81] S.R. Blaszkowski, R.A. van Santen, J. Phys. Chem. B 101 (1997) 2292.
[82] H. Ernst, H. Pfeifer, J. Catal. 136 (1992) 202.
[83] G.A. Olah, A. Molnar, Hydrocarbon Chemistry, Wiley & Sons, New York, 1995.
[84] A. Corma, Chem. Rev. 95 (1995) 559.
[85] C. Tuma, J. Sauer, J. Angew. Chem. 117 (2005) 4847.
[86] M. Haouas, S. Walspurger, F. Taulelle, J. Sommer, J. Am. Chem. Soc. 126 (2004) 599.
[87] S.S. Arzumanov, S.I. Reshetnikov, A.G. Stepanov, V.N. Parmon, D. Freude, J. Phys. Chem. B 109 (2005) 19748.
[88] A. Streitwieser, L. Reif, J. Am. Chem. Soc. 82 (1960) 5003.
[89] J. Huang, Y. Jiang, R.V. Reddy Marthala, Y.S. Ooi, M. Hunger, unpublished results.
[90] H. Foerster, I. Kiricsi, G. Tasi, I. Hannus, J. Mol. Struc. 296 (1993) 61.
[91] J. Huang, Y. Jiang, V.R. Reddy Marthala, W. Wang, B. Sulikowski, M. Hunger, Microporous Mesoporous Mater. 99 (2007) 86.
[92] G.A. Olah, Carbonium Ions, vol. 1, Wiley-Interscience, New York, 1968, pp. 183.
[93] V.B. Kazansky, Catal. Today 51 (1999) 419.
[94] H. Schulz, M. Wei, Microporous Mesoporous Mater. 29 (1999) 205.
[95] W.O. Haag, in: R.A. Bisio, D.G. Olson (Eds.), Proceedings of the 6th International Zeolite Conference, Butterworth, Guildford, 1984, p. 466.
[96] I.M. Dahl, S. Kolboe, J. Catal. 149 (1994) 458.
[97] B. Arstad, S. Kolboe, J. Am. Chem. Soc. 123 (2001) 8137.
[98] (a) P.L. Benito, A.G. Gayubo, A.T. Aguayo, M. Olazar, J. Bilbao, J. Chem. Tech. Biotechnol. 66 (1996) 183;
(b) M. Bjørgen, F. Bonino, B. Arstad, S. Kolboe, K.P. Lillerud, A. Zecchina, S. Bordiga, ChemPhysChem 6 (2005) 232.
[99] (a) M. Hunger, M. Seiler, A. Buchholz, Catal. Lett. 74 (2001) 61;
(b) W. Song, H. Fu, J.F. Haw, J. Am. Chem. Soc. 123 (2001) 4749;
(c) J.F. Haw, W. Song, D.M. Marcus, J.B. Nicholas, Acc. Chem. Res. 36 (2003) 317.
[100] S. Kolboe, Stud. Surf. Sci. Catal. 61 (1991) 405.
[101] J. Melsheimer, D. Ziegler, J. Chem. Soc., Faraday Trans. 88 (1992) 2101.
[102] H.G. Karge, M. Laniecki, M. Ziolek, G. Onyestyak, A. Kiss, P. Kleinschmit, M. Siray, Stud. Surf. Sci. Catal. 49 (1989) 1327.
[103] J. Mohan, Organic Spectroscopy Principles and Applications, Alpha Science International Ltd., Harrow, 2002, pp. 128 and 137.
[104] H.O. Kalinowski, S. Berger, S. Braun, ^{13}C-NMR-Spektroskopie, Georg Thieme Verlag, Stuttgart, New York, 1984, pp. 136.
[105] I. Kirisci, H. Foerster, G. Tasi, J.B. Nagy, Chem. Rev. 99 (1999) 2085.
[106] F.J. Keil, Microporous Mesoporous Mater. 29 (1999) 49.